1

Wireless Power Transfer Applied to NFC

1.1. Introduction

Our knowledge of physics determines four different fundamental forces: two of them produce forces at subatomic distances and govern nuclear interactions, and the other two, gravity and electromagnetism, produce long-range effects. Each can be mathematically described as an electromagnetic field. Michael Faraday was the first to describe one of these forces in 1831. He studied the magnetic field generated around a conductor through which a current flows. A few years later, in the 1860s, James Clerk Maxwell developed and unified the theory of electromagnetism, summarizing it in four equations that now bear his name. However, it was Heinrich Hertz who, in 1887, proved the existence of the electromagnetic waves predicted by Maxwell's equations, inventing the dipole oscillator and the resonator (Buchwald 1994). Radio wave evidence was the beginning of wireless power transfer (WPT), and Nikola Tesla was one of the researchers most involved in this regard. He invented radio frequency resonant transformers (Tesla coils) using inductive and capacitive coupling when trying to develop a wireless lighting system. In 1921, he stated: "Power can be, and at no distant date will be, transmitted without wires, for all commercial uses, such as the lighting of homes and the driving of airplanes. I have discovered the essential principles, and it only remains to develop them commercially." (Wisehart 1921)

Despite the efforts and dedication that Tesla put into WPT, it never achieved commercial success due to the dispersion of wireless power, which mainly depends on the operating frequency and the size of the transmitting antenna. Later, in the

---

Sections of this chapter have been taken from a previous publication by the authors of this book. © 2019 IEEE. Reprinted, with permission, from Boada, M., Lazaro, A., Villarino, R., Girbau, D (2019). Battery-less NFC sensor for pH monitoring. *IEEE Access*, 7, 33226–33239. doi: 10.1109/ACCESS.2019.2904109.

1960s, after knowledge had been acquired of working at microwave frequencies, during World War II, where the energy could be focused into a narrow beam, a new era of WPT began (Brown 1984, 1996).

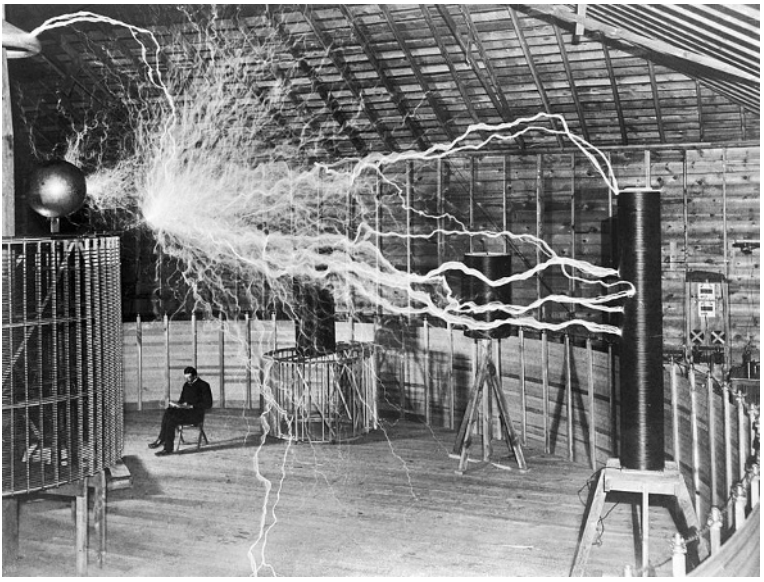

Figure 1.1. *Nikola Tesla in his laboratory in 1899. Image by Dickenson V. Alley, licensed under CC BY-SA 4.0*

Nowadays, three different methods for WPT using electromagnetic fields are employed: inductive coupling, resonant coupling and far field (Shinohara 2012) (see Table 1.1). These three technologies are similar, and they all follow Maxwell's equations. However, each of them has its own characteristics and design constraints.

	Inductive coupling	**Resonant coupling**	**Far field**
Field	Magnetic field	Resonance (magnetic, electric, EM)	EM
Method	Coil	Resonator	Antenna
Distance	Short	Medium	Short to long
Efficiency	Low to high	High	High
Power	High	High	Low to high
Uses	Felica cards, Qi standard (mobile phone charging)	NFC, eZone (mobile phone charging)	Far-field RFID

Table 1.1. *Characteristics of different WPT methods*

Inductive coupling (Figure 1.2(a)) is based on Ampere's circuital law and Faraday's law of induction. The first describes the magnetic field generated by an electrical current passing through a loop (coil) and vice versa; the second predicts the interaction between a time-varying magnetic field and an induced electromotive force. The efficiency of the transmitted power depends on the coupling coefficient, which depends on the distance between the transmitter and receiver. It is used for short-range applications, usually working with frequencies of a few megahertz. This method was the first WPT technology applied to real applications (Flack *et al.* 1971; Akin *et al.* 1998; Peng *et al.* 2010).

Resonant coupling (Figure 1.2(b)) has been widely applied to microwave band-pass filters (BPF) (Cohn 1958; García-García *et al.* 2004); however, it was not until 2007 when researchers from the Massachusetts Institute of Technology (MIT) demonstrated its use for WPT achieving up to 40% efficiency over more than 2 m (Kurs *et al.* 2007; Wei *et al.* 2014). A resonator is composed of a coil (L) and a capacitor (C), and the transmitted power is mainly magnetic. Resonators are currently used in smartphones and other mobile devices.

Unlike inductive and resonant coupling, WPT via radio waves (Figure 1.2(c)) uses the radiated electromagnetic field. Therefore, it uses antennas instead of coils. It is mainly used in far-field RFID systems (Shinohara 2014). It achieves lower power transfer but a much longer range.

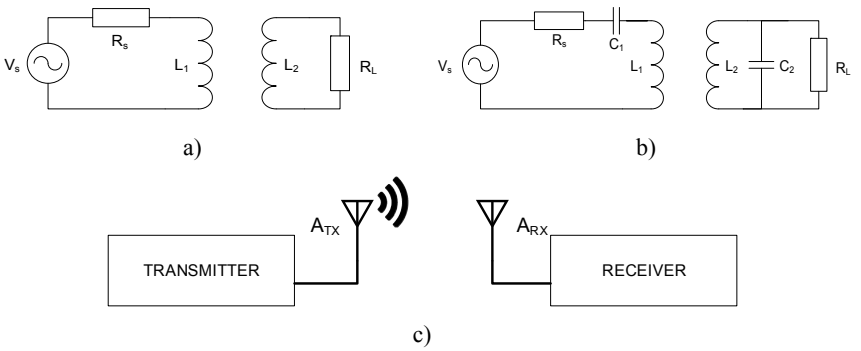

Figure 1.2. *Methods of WPT. (a) Inductive coupling; (b) resonant coupling; and (c) far field*

Resonant coupling, which is the technique used in NFC systems, relies on the principle that resonant objects exchange energy efficiently. To accomplish the power transfer, the source resonator generates an oscillating magnetic field, commonly

working at the MHz range, which is received by another resonator located a few centimeters away. WPT using resonant coupling can be classified according to different parameters (Kim 2012), as shown in Table 1.2.

There are two possible ways to analyze resonant coupling. The first one involves the coupled-mode theory (CMT) (Hamam *et al.* 2007). Conversely, since resonators are based on RLC circuits (see Figure 1.2(b)), the circuit theory – which is more straightforward – can be applied as well and it is the approach used in this chapter.

Classification	Type	Description	Comments
Field used in coupling	Magnetic coupled	Affected by the surrounding permeability	Not affected by the body (medical applications)
	Electric coupled	Affected by the surrounding permittivity	
Power feeding	Direct-fed	Power source and load directly connected to the resonant structure	
	Indirect-fed	Feeding loop	Impedance matching by adjusting the spacing between the resonant structure and the loop
Resonant scheme	Self-resonant	Inductance and capacitance realized by identical structure	
	External resonant	Different structures	Typically the loop structure used for inductance and a capacitor is added

Table 1.2. *Coupled resonant WPT system classification*

1.2. Theoretical background

The underlying physical principles of electromagnetism are needed in order to understand WPT associated with NFC technology, and are briefly reviewed in this section. Inductive coupling consists of a primary coil generating a sinusoidal varying magnetic field, which induces a voltage on the terminals of a secondary coil, thus transferring power to a load. This effect is produced by the fact that a flow of current generates a magnetic field; the magnitude of this field is described as the magnetic field strength and is represented by H. The Biot–Savart law allows the H field

strength and direction to be calculated from any geometry and current, for any point in space (Figure 1.3). Its integral form is given by [1.1]:

$$\vec{H} = \frac{I}{4\pi}\oint_S \frac{d\vec{s} \times \vec{r}}{|r|^3} \quad [1.1]$$

where I is the current, $d\vec{s}$ is a vector along the path S, and r is the point in which the field is being computed.

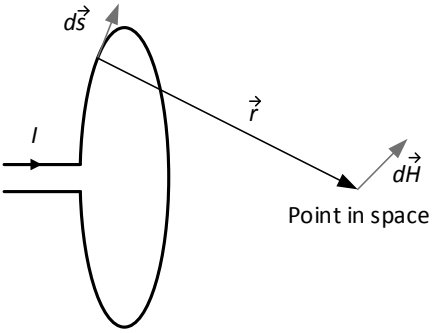

Figure 1.3. *Representation of the Biot–Savart law to measure the* H *field strength in any point of the space. For a color version of this figure, see www.iste.co.uk/girbau/sensors.zip*

For practical applications, the previous integral is not appropriated as closed analytical solutions only exist for special cases. The H field on the center axis of a cylindrical coil is given by (Paret 2016):

$$H = \frac{INr^2}{2\sqrt{(r^2 + x^2)^3}} \quad [1.2]$$

where N is the number of turns, r is the radius of the loop and x is the distance from the center of the coil. Furthermore, when the loop has a rectangular shape, with side lengths a and b, the strength of the magnetic field at distance x is (Paret 2016):

$$H = \frac{INab}{4\pi\sqrt{\left(\frac{a}{2}\right)^2 + \left(\frac{b}{2}\right)^2 + x^2}} \cdot \left(\frac{1}{\left(\frac{a}{2}\right)^2 + x^2} + \frac{1}{\left(\frac{b}{2}\right)^2 + x^2} \right) \quad [1.3]$$

The Biot–Savart law achieves accurate results for the near-field region, and it is used to obtain the homogeneity of the emitted H field and the optimum antenna radius.

The amount of magnetic field that passes through a given surface (Φ) can be measured by:

$$\Phi = BA \quad [1.4]$$

where B represents the magnetic flux density and A is the area of the given surface. The relationship between the flux density (B) and the field strength (H) is given by:

$$B = \mu_0 \mu_r H = \mu H \quad [1.5]$$

being that μ_0 is the vacuum permeability, and μ_r is the relative permeability (μ is the product of μ_0 and μ_r). When using coils of N loops, the total magnetic flux (ψ) is the sum of the flux (Φ):

$$\psi = \sum \Phi_N = N\Phi = N\mu HA \quad [1.6]$$

The relationship between the magnetic flux and the current is the inductance (L), and can be expressed as:

$$L = \frac{\psi}{I} = \frac{N\Phi}{I} = \frac{N\mu HA}{I} \quad [1.7]$$

The physical principle of NFC for communication relies on the mutual inductance between two coils (M_{21}). Mutual inductance defines the effect of the magnetic field generated by the first coil with area A_1 over a second coil, located near the first, with area A_2:

$$M_{21} = \frac{\psi_{21}(I_1)}{I_1} = \oint_{A_2}^{\infty} \frac{B_2(I_1)}{I_1} dA_2 \quad [1.8]$$

where the sub-indices *1* and *2* refer to the first and second coils, respectively, and ψ_{21} is the coupling flux which passes through both coils. Combining Ampere's law and the Biot–Savart law, thus applying the reciprocity theorem, it can be stated that:

$$M = M_{21} = M_{12} \quad [1.9]$$

And the mutual inductance is directly related to the coil inductance by:

$$M = k\sqrt{L_1 L_2} \qquad [1.10]$$

where k is the coupling coefficient.

Figure 1.4 depicts the mutual inductance (M) between two coils.

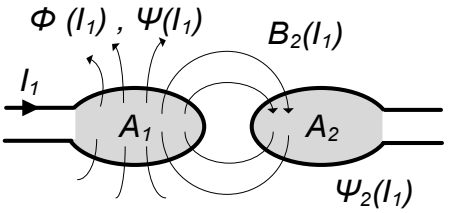

Figure 1.4. *Representation of mutual inductance (*M*) between coils*

This chapter analyzes WPT within the NFC scenario using a smartphone as the reader. Thus, beyond the basic background of WPT that has been explained briefly up to this point, certain specific key constraints such as the resonator design, NFC IC characterization, potential environmental effects and comparison between commercially available NFC chips with energy harvesting (EH) are addressed.

1.3. NFC systems

This section describes the reader and the tag and proposes both a system model and a procedure to understand, analyze and design WPT in NFC systems, when using a smartphone as the reader to connect to standardized NFC tags. In this context, the reader cannot, therefore, be modified and the NFC antenna depends on the smartphone used.

1.3.1. *Reader model*

Figure 1.5 shows the schema of the reader. It includes a model for the reader IC, an electromagnetic interference (EMI) filter and a matching network. The reader consists of a voltage source (V_{out}) which is connected to the EMI filter through a resistance (R_{out}). The EMI filter is a low-pass filter. Its function is reducing the second and the higher harmonics and performing an impedance transformation. This filter is composed of two resistors (R_0), two inductors (L_0) and two capacitors (C_0).

Two capacitors (C_s) are used as the matching network to match the impedance between the EMI filter and the antenna.

Two resistors (R_x) and a capacitor (C_{in}) compose the receiver circuit to adjust the received power levels, avoiding its saturation. The antenna is modeled as an inductance (L_1) in series with a resistance (R_a) and a capacitance (C_a). C_p is the parasitic capacitance of the antenna. Two resistors (R_Q) may be added between the antenna and the matching network in order to reduce the quality factor (Q) and to meet with the standard requirements.

As is also shown in Figure 1.5, the reader can be modeled using a Thevenin equivalent circuit with a voltage source and an output impedance (R_s). This simplified model is useful for inserting the transmitter in circuit simulators. A series capacitance (C_1) is added to make the circuit resonant at the operating frequency. The parasitic capacitance of the reader antenna (C_p) in the matching network has been considered and is included in the equivalent Thevenin model. An equivalent model can be used for the reader antenna, which is modeled as an inductance (L_1) and its losses (R_1, including R_Q) in series with the inductance. The reader includes a matching network, so a perfect match is assumed at the resonance frequency, $R_s = R_1$.

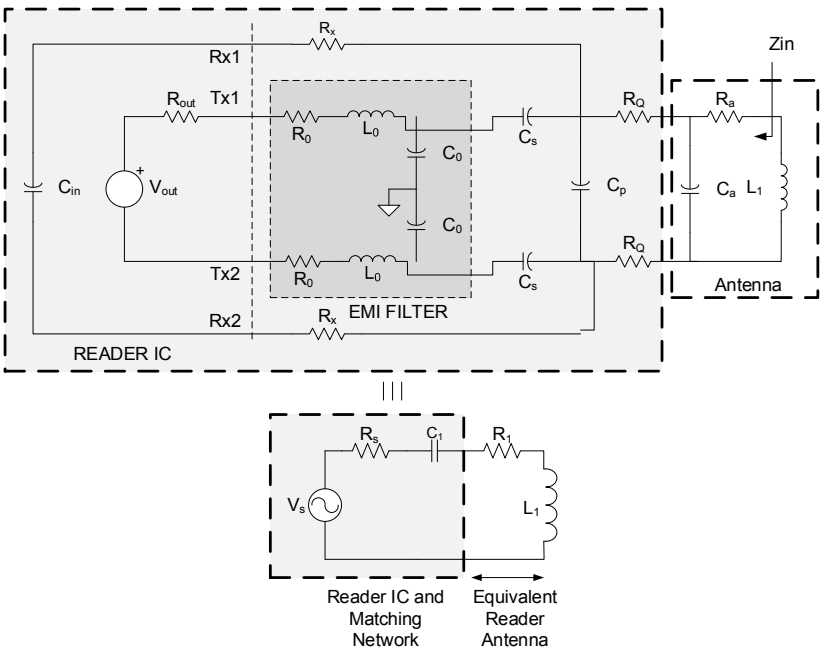

Figure 1.5. *Circuit model of the reader, including the matching network (top) and the simplified circuit model (bottom)*

It is known that in some applications the reader correctly communicates with a smart card at a large distance but not at short distances, independently of the demodulation quality of the backscattered signal (Jiang *et al.* 2005; Marechal and Paret 2008). This phenomenon is known as the loading effect, resulting in a lack of transmitted power due to the strong influence of the tag's load on the reader (Jiang *et al.* 2005; Marechal and Paret 2008).

In addition, when using a smartphone as the NFC reader, unlike other WPT systems, the transmitted power and reader antenna topology depend on the mobile model. Typical transceiver IC for NFC in commercial smartphones can achieve transmitted powers of between 20 and 23 dBm (e.g. NXP PN7120 (NXP Semiconductors 2018b) or TI TRF7970A (Texas Instruments 2014b) IC transceivers).

1.3.2. *Tag model*

Figure 1.6 shows the block diagram of an NFC tag IC. There are two main blocks connected to the antenna (Lu *et al.* 2016). The first is the WPT unit, and it has the function of harvesting the energy to power up the IC; while the second is the communication unit that demodulates the data and generates the clock for the transmission of information back to the reader. This chapter focuses on the WPT unit. This is composed of an RF limiter, a rectifier, a shunt regulator and a load modulator, which can be modeled as a shunt capacitance with the antenna.

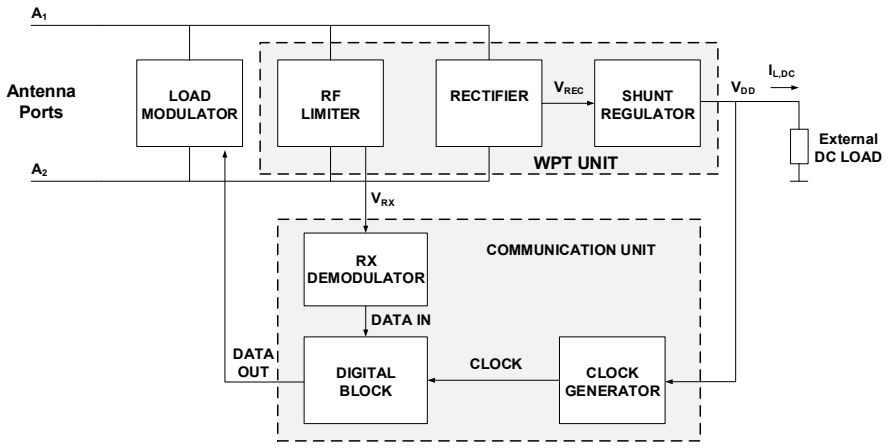

Figure 1.6. *Block diagram of the NFC tag IC*

Due to its proximity to the reader, the coupled AC signal at the antenna can be large, which could lead to the destruction of the MOS transistor. Therefore, an RF limiter is needed to prevent internal circuit damage caused by any undesired high-input signal. Then, the AC signal is translated into a DC signal by means of a full-wave rectifier. The rectified DC voltage is regulated in order to obtain a stable voltage for the operation of the communication unit.

For modeling the limiter, the circuit described in Lu, Li and Lin (2016) and shown in Figure 1.7 is considered. This limiter is based on two large-area NMOS shunt transistors that are activated when the input power is enough to produce a current through the diodes that is larger than the threshold voltage needed to activate the transistors. The limiter is also used to implement an envelope detector using the diodes and the *RC* filter (R_1 and C_1) for ASK demodulation. The output of this circuit (V_{Rx}) is connected to the input of a slicer circuit for data demodulation.

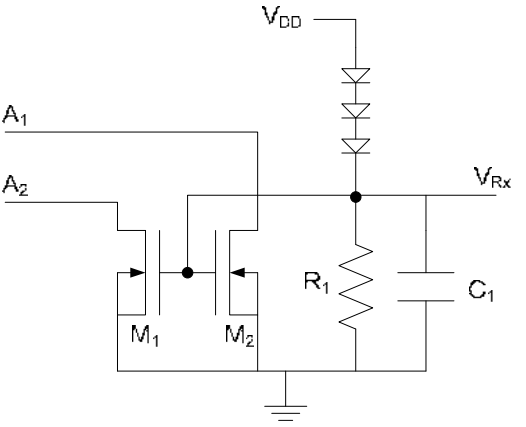

Figure 1.7. *RF limiter model inside the NFC IC*

A high-efficiency rectifier is required for the RF-to-DC conversion. This is often based on a full-wave bridge rectifier in which the diode pairs turn on during each cycle of the AC signal. However, efficiency is limited for the threshold voltage of the diodes. Schottky diodes can be used in this topology to reduce these voltage drops, but these devices are not compatible with the conventional CMOS technology. Several CMOS-based rectifiers have been proposed in the literature. The most frequently used are the NMOS bridge and the CMOS gate cross-coupled (or cross-connected) rectifier (Jamali *et al.* 2005) (Figure 1.8).

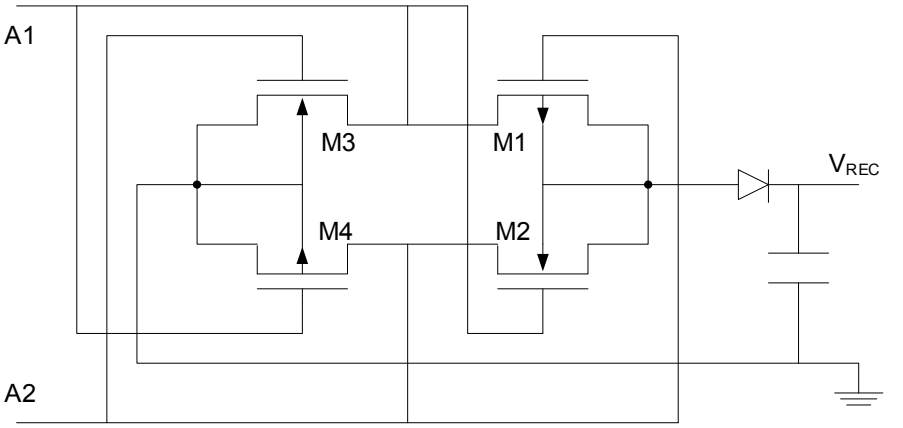

Figure 1.8. *Model of the full-wave rectifier based on the CMOS gate cross-coupled rectifier*

A shunt regulator can be used to model the regulator in the simulation (e.g. based on a zener diode). Although lateral zener diodes can be implemented in standard CMOS processes (Teichmann *et al.* 2003), the shunt regulator is often implemented with transistors. Nevertheless, all the topologies are based on the same principle which consists of reducing the shunt resistance of a bypass transistor when the input voltage is higher than the desired output voltage. Figure 1.9 shows the shunt regulator used in this analysis (Zhu 2004; Jiang *et al.* 2005; Hu *et al.* 2009). In this circuit, the shunt impedance to reduce the voltage is controlled comparing a bandgap-based reference voltage and the output voltage.

The load modulator (Figure 1.10) is formed by two NMOS transistors that act as switches, each of them connecting one capacitor from the RF input to ground (Jianguo *et al.* 2007; Alcalde *et al.* 2014). In order to transmit the information to the reader, the transistors are switched ON and OFF by the data signal connected to the gate (DATA OUT), which results in a load impedance change at the antenna as a function of the data. Since this analysis focuses on the WPT, the effect of the modulator is included in the shunt parasitic capacitance of the IC.

The proposed simplified model for the tag is shown in Figure 1.11. The tag IC is modeled as a resistance (R_{IC}) in parallel with a capacitor (C_{IC}). The tag antenna is modeled as an inductance (L_2) connected in series with a resistance (R_2). A shunt parasitic capacitance of the tag antenna (C_p) is also included. Finally, a tuning capacitance C_{tun} is added to make the circuit resonant at the operating frequency.

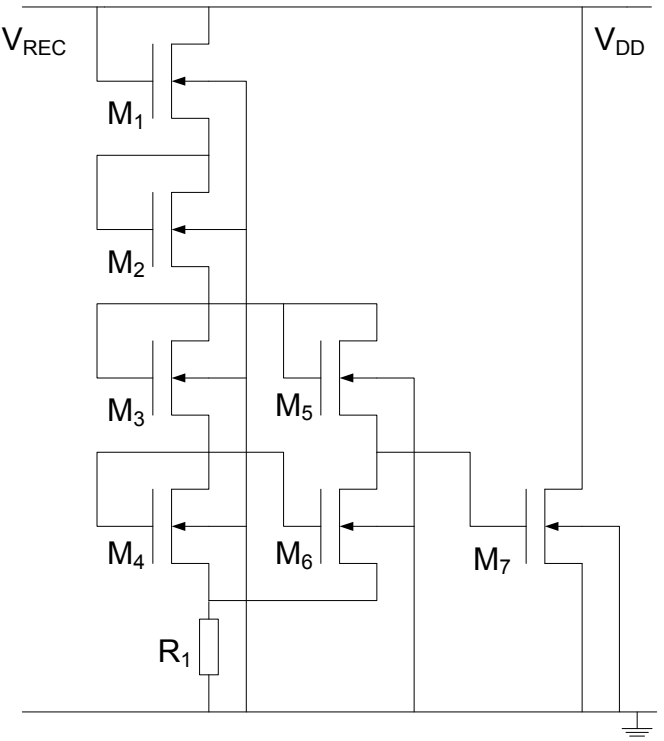

Figure 1.9. *Shunt regulator circuit model*

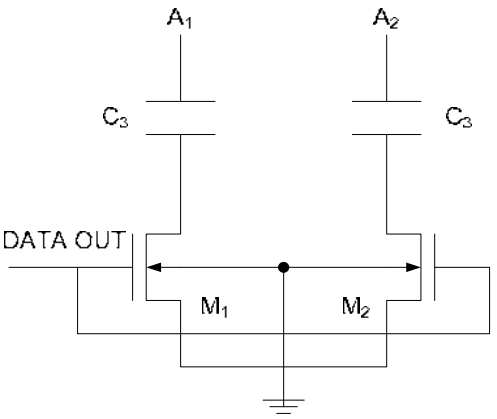

Figure 1.10. *Load modulator model formed by two NMOS transistors*

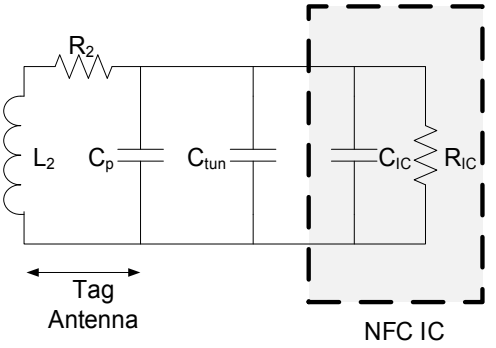

Figure 1.11. *Simplified circuit model of the tag including the tag antenna, tuning capacitor and NFC IC*

An important point to consider is that the IC impedance presents a nonlinear behavior; thus, the impedance at the operating frequency changes depending on the received power. However, it is not easy to measure this nonlinearity. The impedance of RF laboratory equipment is usually 50 Ω, and the IC of the tag is expected to have high impedance (in the order of kΩ). The second consideration at this point is the high-power level required, comparable to the real power levels generated by the reader. In Gvozdenovic *et al.* (2014), a high-power method for the impedance characterization of HF RFID chips is proposed, by using the shunt or series method, measuring the transmission coefficients (S_{21}) using a series setup. This method improves the accuracy obtained by the reflected method (measuring S_{11}) (Gebhart *et al.* 2010), since the latter is less reliable when measuring high impedance chips. As shown in Gvozdenovic *et al.* (2014), HF RFID transponders behave in a strong nonlinear way when the received power increases.

1.3.3. *NFC system model*

Figure 1.12 groups together the reader and tag models introduced in the preceding sections, showing the proposed simplified circuit model of the WPT between the reader and the tag. The reader includes the IC model followed by its matching network and antenna. The tag is modeled as an antenna, a tuning capacitor and the IC model. The energy transfer between both elements depends on the coupling coefficient (k) that will be explained later in this chapter.

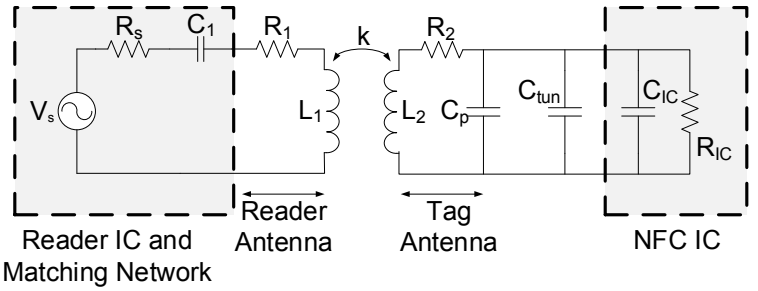

Figure 1.12. *Wireless power transfer model between the reader and the tag*

1.4. NFC constraints

Even though a device with NFC technology (reader) can transmit power wirelessly to power up a receiver (tag), its main purpose is the data transfer. Furthermore, with the incorporation of this technology in most of the smartphones manufactured today, the methods to apply it encompass a huge variety of solutions, with different antenna sizes and materials, as well as different emission power levels and electrical characteristics. Unlike other specific WPT systems which are specifically designed for the purpose of transferring power wirelessly, a number of additional restrictions must be taken into account when developing NFC devices, thus allowing an efficient power transfer and ensuring a correct data transfer, regardless of the reader used, which cannot normally be modified (especially when using smartphones), and imposes several restrictions that must be taken into account during the tag and system design.

1.4.1. *Antenna design*

As in any wireless communication system, NFC needs an antenna to establish communication between the transmitter and the receiver. In addition, when WPT is considered, not only to feed the tag for communicating but also for feeding additional electronics and sensors, it is crucial to ensure the maximum power transfer through the antennas. This section describes the main parameters to consider for their design.

1.4.1.1. *Resonance frequency (f_r), operation frequency (f_o) and antenna tuning*

The NFC nominal operation frequency (13.56 MHz) is denoted as f_0. The resonance frequency (f_r) of the antenna is the frequency at which the inductive and

capacitive reactances cancel each other out, thus behaving as purely resistive. Note that, in some cases, the angular frequency (ω) is also addressed, which is related to the frequency as $\omega = 2\pi f$. To optimize power and data transfer, it is essential to adjust the resonance frequency (f_r) of the antenna to the operation frequency (f_0) of the system; this process can be done by tuning the antenna. However, it may be necessary to tune it to a slightly higher frequency when considering the change in frequency caused by environmental conditions, such as the tag material or the presence of metallic objects, as for instance a metallic reader enclosure, when working in very short ranges. The presence of a metal near the coil produces eddy currents in the opposite direction of the generated field, absorbing part of the power. This metal introduces a capacitance on the antenna impedance and reduces its inductance, which makes the energy to partially reflect at the antenna terminals since it is not matched to the input impedance.

If we take into consideration the circuit model of the loop antenna shown in Figure 1.13, the reduction of the tag antenna inductance (L_a) and changes in the parasitic capacitance (C_p, which includes parasitic antenna capacitance and parasitic capacitance due to interconnections), the resonance frequency of the antenna f_r can be written as:

$$f_r \approx \frac{1}{2\pi\sqrt{L_a\left(C_{IC} + C_p + C_{tun}\right)}} \qquad [1.11]$$

where C_{IC} is the internal IC capacitance and C_{tun} is the capacitor used to adjust the resonance frequency (f_r) to the operation frequency f_0 (13.56 MHz). The resonance frequency of a loop antenna can be measured by connecting another loop antenna to a vector network analyzer (VNA), approaching it to the loop antenna to be tested and obtaining the S_{11} parameter. The antenna connected to the VNA and the antenna to be measured should not be approached too much in order to avoid loading effects, it should be placed just close enough to be slightly coupled and to detect the resonance from the S_{11} measurement.

As mentioned before, the operation frequency of NFC is f_0 = 13.56 MHz, which leads to a wavelength of about 22 m ($\lambda = c/f_0$, where $c \approx 3 \cdot 10^8$ *m/s*). This leads to a half-wave dipole antenna of 11 m, which is not suitable for a handheld or a smartcard. The antenna used is much smaller; therefore, the radiation efficiency is small, and the typical parameters measured in antennas, such as the gain or the radiation pattern, are not relevant. An NFC antenna is basically a loop-shaped inductor, as shown in Figure 1.13, and its performance depends mostly on the loop area (A) and the number of turns (N). As a general rule, the larger the area and the more turns it has, the better its performance. R_p is the parasitic resistance, the inductance (L_a) is mainly defined by the number of turns of the loop, the resistance

(R_a) by the diameter and total length of the loops and the capacitance (C_p) by the separation between the antenna loops and the number of turns.

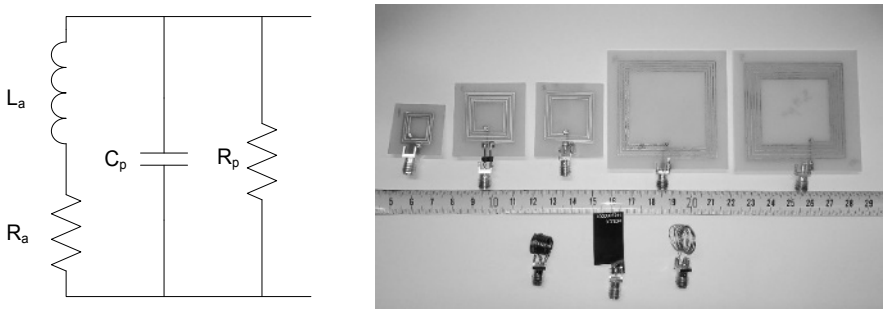

a) b)

Figure 1.13. *(a) Circuit model for a loop antenna and (b) antennas of different sizes and numbers of turns. For a color version of this figure, see www.iste.co.uk/girbau/sensors.zip*

The theoretical inductance for a rectangular wire coil can be calculated from (Jacobi and La Cost 2017):

$$L_a = N^2 \frac{\mu}{\pi}\left[-2(w+h) + 2\sqrt{h^2+w^2} - h\ln\left(\frac{h+\sqrt{h^2+w^2}}{w}\right) - w\ln\left(\frac{w+\sqrt{h^2+w^2}}{h}\right) + h\ln\left(\frac{2h}{a}\right) + w\ln\left(\frac{2w}{a}\right)\right] \quad [1.12]$$

where N is the number of turns, w and h are the average width and height of the coil, respectively, and a is the PCB width. The inductance can be measured from the Z parameters as: $L_a = Im(Z)/w_0$.

The easiest way to precisely calculate L_a and R_a is by connecting the coil antenna to a VNA and then calculating the impedance of the antenna (Z_{11}) from the measured S_{11} parameter at the operation frequency (f_0), knowing that (NXP Semiconductors 2018a):

$$Z_{11} = R_a + j2\pi f_0 L_a \quad [1.13]$$

The values of resistance and inductance are usually given by the VNA; however, the capacitance is not measured but can be estimated using the equation (NXP Semiconductors 2019):

$$C_p = \frac{1}{(2\pi f_r)^2 L_a} \quad [1.14]$$

A series equivalent total resistance of the antenna (R_T) at the operation frequency (f_0), which combines the antenna and parasitic resistances (R_a and R_p, respectively), can be calculated by first measuring the equivalent resistance at the resonance frequency ($R_{p(fr)}$) with the VNA, and using its value to measure the parallel equivalent resistance at f_0 ($R_{p(f0)}$):

$$R_{p(f_0)} = \frac{R_{p(f_r)}}{\sqrt{\frac{f_0}{f_r}}} \quad [1.15]$$

and then calculate R_T using:

$$R_T = R_a + \frac{(2\pi f_0 L_a)}{R_{p(f_0)}} \quad [1.16]$$

The parasitic resistance (R_p) can be calculated using the following expression (NXP Semiconductors 2019):

$$R_p = \frac{(2\pi f_0 L_a)^2}{R_a + 2R_Q} \quad [1.17]$$

where R_Q is the damping resistor used to adjust the quality factor (defined and explained in equation [1.28]).

1.4.1.2. *Antenna factor (AF)*

The magnetic antenna factor (AF) at a determined frequency (f) is defined as the ratio between the incident magnetic field (H) and the output voltage at the load (V_o) (Ishii and Komiyama 2004):

$$AF(f) = \frac{H(f)}{V_o(f)} \quad [1.18]$$

The AF of the coil antenna is used to measure the average magnetic field in the tag. In order to obtain the AF of the antenna, the circuit of Figure 1.14 can be used.

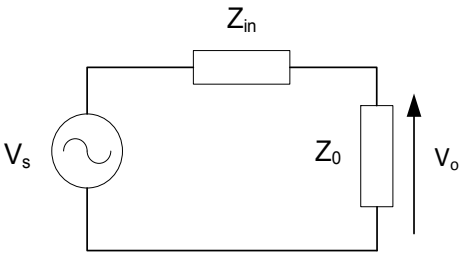

Figure 1.14. *Circuit considered to obtain the* AF

Taking into account Faraday's law: $V_s = -j\omega\pi a^2 \mu_0 H$, where a is the radius of the antenna, and knowing that $V_0 = (Z_0/(Z_{in} + Z_0))V_s$, Z_{in} being the antenna impedance and Z_0 being the reference impedance (50Ω), the AF can be obtained from the measured antenna impedance as (Ishii and Komiyama 2004):

$$AF = \frac{Z_0 + Z_{in}}{j2\pi f \mu_0 Z_0 A \cdot N} \quad [1.19]$$

where A is the loop area and N is the number of turns of the loop.

1.4.2. *Coupling coefficient (*k)

The coupling coefficient (k) of a pair of coils (C_1, C_2) is a measure of the magnetic field transferred between them and therefore it is a fundamental parameter in NFC. It depends on the shape of the antennas, the distance and alignment between them, and the materials. The coupling coefficient can be calculated, as shown in expression [1.20], from the Z parameters either obtained from electromagnetic simulation or from the S parameter measurement performed with a VNA (Zargham and Gulak 2012)

$$k = \frac{M}{\sqrt{L_1 L_2}} = \frac{\sqrt{Im(Z_{12}) \cdot Im(Z_{21})}}{\sqrt{Im(Z_{11}) \cdot Im(Z_{22})}} \quad [1.20]$$

It is known that the maximum coupling coefficient between two coils is obtained when the radius of the coils is identical (Zierhofer and Hochmair 1996; Lazaro *et al.* 2018). However, NFC antennas (especially in the reader side) are embedded in a large variety of devices, and each of them uses a different antenna configuration. This factor must be considered when designing NFC tags.

1.4.3. *Quality factor (Q)*

The quality factor (Q) of a resonator determines its bandwidth. It depends on the relationship between the imaginary and real parts of its impedance Z. It can be expressed as:

$$Q = \frac{Im(Z)}{Re(Z)} \quad [1.21]$$

The relationship between the quality factor at the resonance frequency (f_r) and the bandwidth (BW) can be described as:

$$BW = \frac{f_r}{Q} \quad [1.22]$$

A high value of Q at the transmitter (reader) is translated into a narrow band, as can be seen in Figure 1.15, which benefits the power transfer. However, to ensure that the sidebands, produced by the backscattering modulation containing the information, are correctly received by the reader, the standards determine a maximum Q factor.

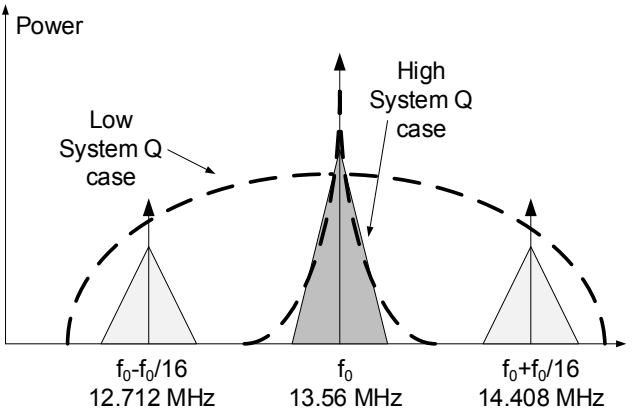

Figure 1.15. *Frequency spectrum of the NFC system with the carrier frequency (f_0) and the sidebands*

The maximal Q of a transmitter depends on the subcarrier frequency and the type of coding used. In the worst-case scenario (ISO/IEC 14443A), a maximal value of Q is $f_0/(2\ x\ bit\ rate)$, which, at a bit rate of 106 kbps, leads to a maximum Q of 64. ISO/IEC 15693 allows higher values of Q, and its maximum value comes from the

pause on the carrier frequency (T_p, depicted in Figure 1.16) such as $Q_{max} = f_0 \times T_p$, being $T_p = 9.44\ \mu s$; thus, $Q_{max} = 128$. It is important to mention that the quality factor of printed antennas usually has a Q higher than that required by the standards; therefore, a series resistor is added in order to reduce it (included in R_1 in Figure 1.12, which models the antenna resistance and this series resistance).

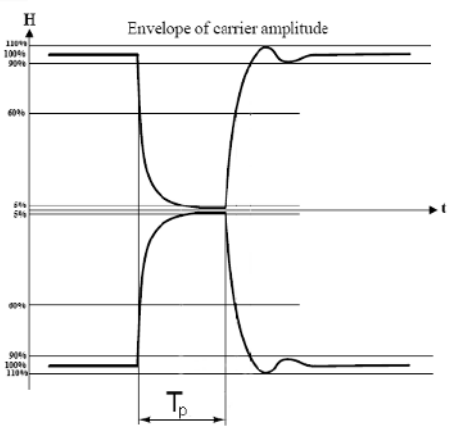

Figure 1.16. *ASK with a 100% modulation envelope amplitude.* T_p *is the protocol pause time, which determines the maximum* Q

Three different Q's can be defined for each side (reader and tag): the antenna quality factor (Q_i), the quality factor of the load (i.e. the NFC IC, Q_L) and the total quality factor of the whole transponder (Q_{iL}). The unloaded quality factor of the coil i (being i = 1 for the reader, and i = 2 for the tag) is obtained from the inductance and resistance at the angular resonance frequency (ω_0) with [1.21]. The total quality factor (Q_{iL}) is computed from:

$$Q_{iL} = \frac{Q_i Q_L}{Q_i + Q_L} \qquad [1.23]$$

where the external quality factor (Q_L) is:

$$Q_L = \frac{R_{IC}}{\omega_0 L_i} \qquad [1.24]$$

where $i = 1{,}2$, and corresponds to the component values in Figure 1.12.

Analogously to the case of the transmitter, the total quality factor of the tag (Q_{2L}) is limited to avoid degradation of the modulation of the subcarrier. Therefore, the

maximum value of Q_{2L} is approximately $Q_{2L,max} = 8\pi \approx 25$ (Gebhart 2011). A higher quality factor would increase the time constants for the transition and decrease the load modulation. This limitation is not present in WPT systems devoted to wireless charging. The total quality factor of the tag (Q_{2L}) is given by the hyperbolic average of the quality factor of the tag antenna (Q_2) and the quality factor associated with the IC impedance (Q_L). Thus, the quality factors of the tag are defined by:

$$Q_2 = \frac{\omega_0 L_2}{R_2} \quad [1.25]$$

$$Q_L = \frac{R_{IC}}{\omega_0 L_2} \quad [1.26]$$

$$Q_{2L} = \frac{Q_2 Q_L}{Q_2 + Q_L} \quad [1.27]$$

As mentioned above, the Q factor of an antenna depends on its inductance and series resistance (normally small), and, since standards determine a maximal value of Q, it is common to add two dumping resistors (R_Q) at each side of the antenna to reduce the quality factor. The value of such resistors can be calculated to reach the desired value (Q_{des}) with the following equation (NXP Semiconductors 2019):

$$R_Q = 0.5\left(\frac{\omega_0 L_a}{Q_{des}} - R_a\right) \quad [1.28]$$

The maximum quality factor to ensure the bandwidth required for the backscattering communication (Q_{2L}) is given by:

$$R_{IC} < \omega_0 L_2 Q_{2L,max} \quad [1.29]$$

1.4.4. *Efficiency (η)*

The efficiency (η) in WPT is defined as the ratio between the power on the load (P_L) and the emitted power (P_{in}). In the case of NFC, it depends on the coupling coefficient (k) between the coils, and the quality factor (Q) of each element, according to the following expression:

$$\eta = \frac{P_L}{P_{in}} = \frac{k_{12}^2 Q_1 Q_{2L}}{1 + k_{12}^2 Q_1 Q_{2L}} \cdot \frac{Q_{2L}}{Q_L} \quad [1.30]$$

where k_{12} is the coupling coefficient between coils 1 and 2, and Q_1, Q_L and Q_{2L} are the quality factors of the reader antenna, the tag NFC IC and the whole tag, respectively. It is important to notice that the magnetic coupling efficiency is very sensitive to primary–secondary coil alignment and distance, since the magnetic field decays as $1/r^3$, r being the distance between coils.

1.4.5. *Average magnetic field (H_{av})*

The average magnetic field (H_{av}) is obtained from the root-mean-square voltage (V_{RMS}) calculated from the measured power (using a spectrum analyzer (SA)) at the carrier frequency from the antenna terminals. This parameter, as the name suggests, determines the magnetic field received at the antenna, and is calculated from the voltage generated on the coil terminals and the AF; thus, it depends on the electrical and geometrical parameters of the antenna. It can be obtained as:

$$H_{av}(A_{RMS}/m) = V_{RMS} \cdot |AF| \qquad [1.31]$$

1.4.6. *Environmental effects*

The magnetic and electric fields with a ground plane directly below are greatly degraded (Huang 2010). The presence of a metal close to the antenna produces eddy currents which create a magnetic field in the opposite direction, absorbing power and detuning the antenna due to a decrease in its inductance and quality factor. Considering that the most common readers used in NFC are smartphones, which usually have a metallic enclosure, or, in some cases, place the antenna over the battery surface, this situation must be taken into account. The most common way to deal with this undesired effect is to put a sheet of a high-permeability material between the antenna and the ground plane, thus creating a shield. Ferrite is the material normally used for this purpose, to help isolate the antenna. However, it does not completely eliminate the effect of the metal surface since only part of the magnetic flux will be conducted through the thin foil of ferrite, as depicted in Figure 1.17.

Another particular case is the design of tags for medical applications, where the tag is placed on the skin or is implanted. It is important to note that the inductance (L_a) is not affected by the dielectric material and is therefore unaltered when the antenna is implanted on the body. However, implantable devices must use a coating layer to isolate the electronics from the body. This is commonly done by using silicon rubber due to its high chemical inertness and durability. The capacitances introduced by the coating layer must be taken into account and this is included as C_s

in the circuit model of Figure 1.18. In addition, the series resistance (R_a) is frequency-dependent, mainly due to the skin effect. The conductivity of biological tissue is much smaller than that of the metal used for the coil strips, so the eddy current generation in the tissue is negligible.

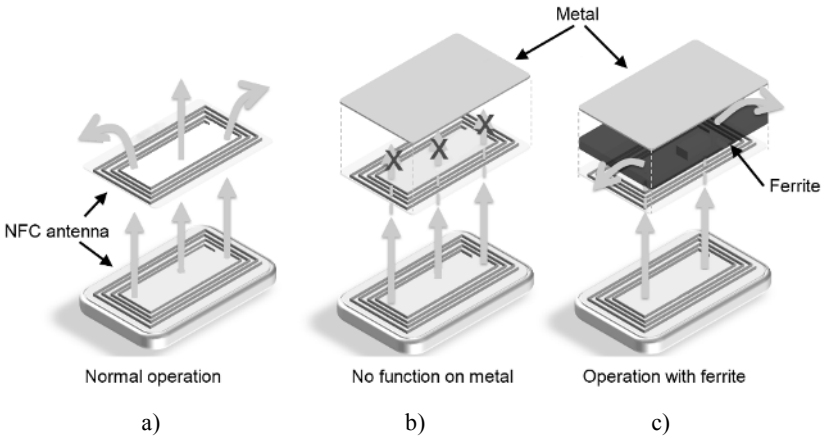

Figure 1.17. *Presence of a metal close to the antenna. (a) Normal operation; (b) field affected by a metal; and (c) use of ferrite sheet. For a color version of this figure, see www.iste.co.uk/girbau/sensors.zip*

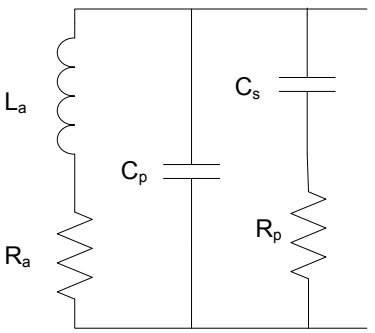

Figure 1.18. *Circuit model for an implanted loop antenna*

1.5. NFC simulation and measurement

The aim of this section is to develop the concepts and theory outlined above using simulation tools and measurement equipment. A number of practical methods

are used to measure the magnetic field and the coupling coefficient. The different antenna topologies and materials are classified, as well as the different types of readers and ICs of the tag, highlighting in the latter its EH capacity, as well as the configurations used to characterize it, with the purpose of giving a general overview of the processes used for analyzing the performance and viability of the tags and applications presented in the next chapters.

Most of the measurements presented in this book have been done using a Xiaomi Mi Note 2 smartphone as a reader. The NFC antenna of this model is placed on a metallic cover that protects the circuitry of the phone and is located around the camera. The reader antenna is shown in Figure 1.19 and consists of five loops, shielded by a high-permeability material sheet (ferrite sheet).

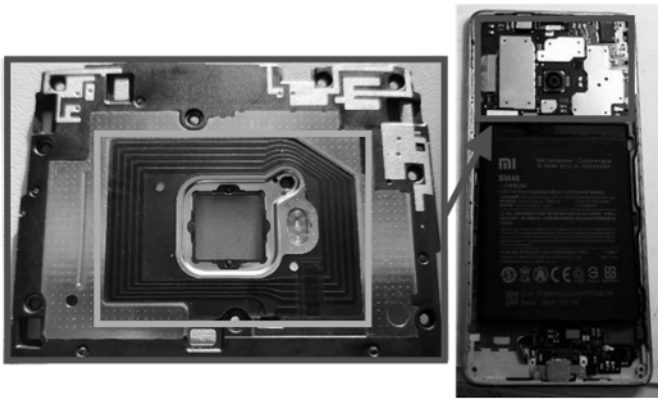

Figure 1.19. *Back of the Xiaomi Mi Note 2 (right) and the NFC antenna (green square). For a color version of this figure, see www.iste.co.uk/girbau/sensors.zip*

1.5.1. *Magnetic field (H_{AV})*

An automatized setup to measure the magnetic field received at the antenna is shown in Figure 1.20. It is composed of the reader (commercial smartphone, placed on a moving part controlled by a stepper motor, Nema 24), the antenna under test, which is connected to a vector network analyzer (VNA, Agilent E5062A) or to a spectrum analyzer (SA, Rhode & Schwarz FSP) by means of the SPDT (single-pole-double-throw) switch MSP2T-18 from Mini-Circuits, which is governed by a voltage supply (Agilent E3631A). The SA, the VNA and the power supply are connected to a computer via the general-purpose instrumentation bus (GPIB), and the stepper motor via the universal serial bus (USB). The procedure to control the instruments is programmed using a MATLAB script, first selecting the appropriate voltage on the

power supply to select the switch output, choosing the VNA to measure the S_{11} parameter, and then the SA to measure the power received at the operation frequency (f_0, 13.56 MHz). Once the readings from the VNA and the SA are done, the stepper motor moves the reader 1 mm, and the process is repeated for a selected range of distances.

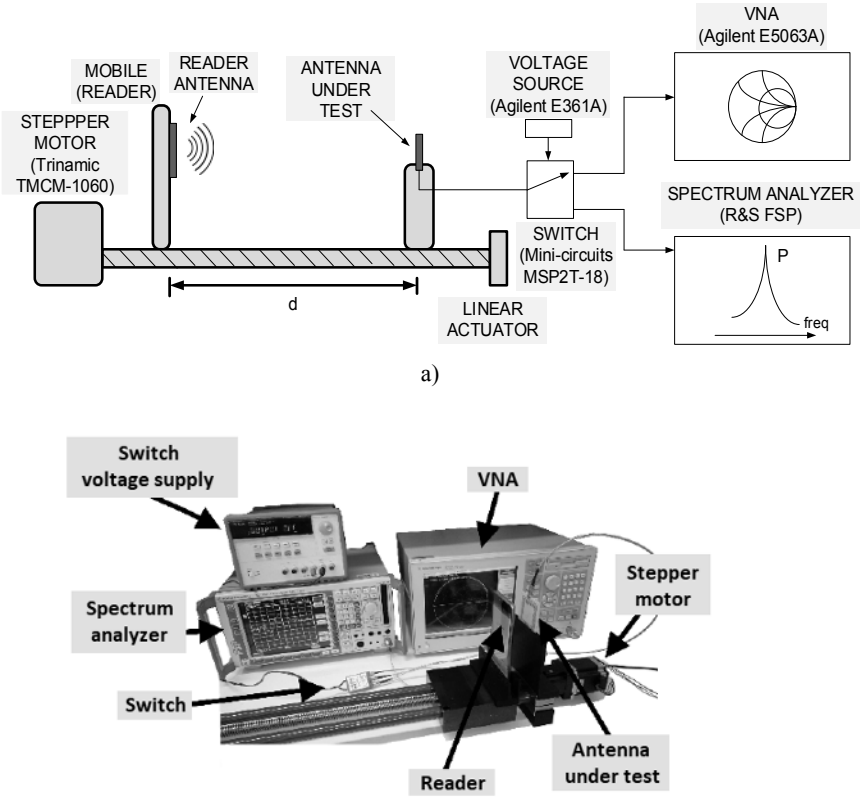

Figure 1.20. *Setup to measure the magnetic field, block diagram (a) and photograph (b). The system is composed of a reader (smartphone), an antenna under test, a spectrum analyzer, a vector network analyzer, an SPDT switch and voltage supply. For a color version of this figure, see www.iste.co.uk/girbau/sensors.zip*

The performance is analyzed by measuring the reflection coefficient (S_{11}) of the antenna at each distance (d), which is used to calculate the AF. The AF is multiplied

by the power received (V_{RMS}) (Figure 1.21(a)) to measure the received magnetic field (H_{av}) (Figure 1.21(b)). From the S parameters, it is possible to calculate the Z parameters which are used to calculate the inductance (L_2) (Figure 1.21(c)) and quality factor (Q_2) (Figure 1.21(d)) for different distances. The plots of these parameters shown in Figure 1.21 are obtained for a six-loop coil antenna, with an area of 50×50 mm, manufactured on FR4, and using a Xiaomi Mi Note 2 as a reader. It can be observed that the inductance and quality factor decrease due to the proximity of the metallic mobile. This effect is studied in detail in section 1.5.3.

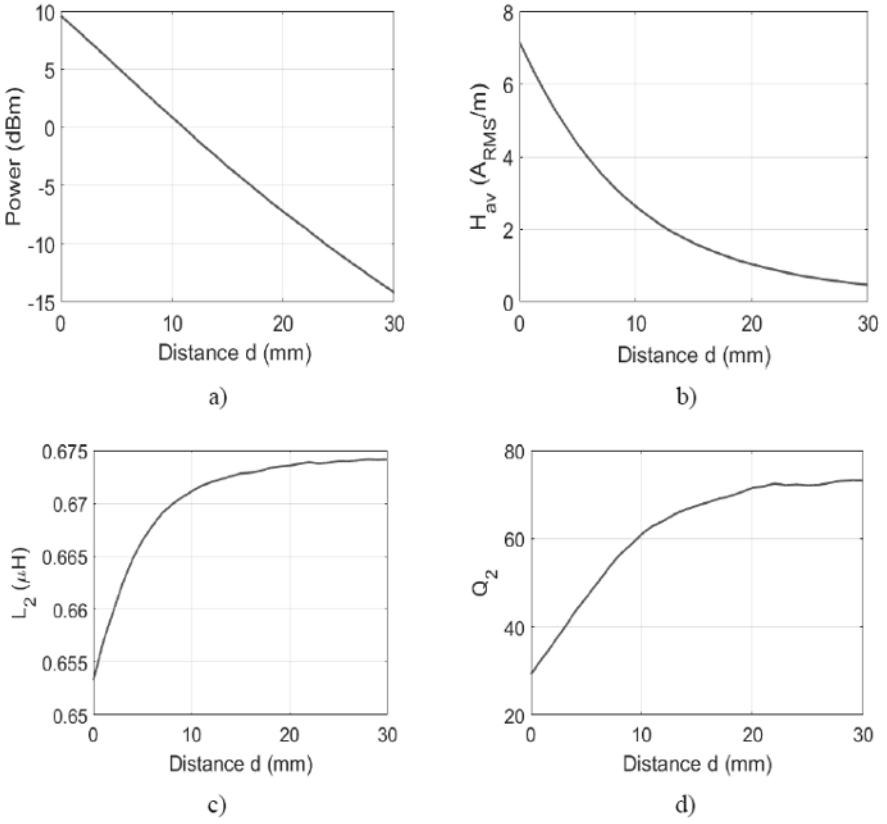

Figure 1.21. *Magnetic field measurements of a coil antenna as a function of distance using a Xiaomi Mi Note 2 as a reader. (a) Power received; (b) magnetic field received (Hav); (c) inductance (L_2); and (d) quality factor (Q_2). For a color version of this figure, see www.iste.co.uk/girbau/sensors.zip*

1.5.2. *Coupling coefficient (k)*

In order to evaluate the behavior of the coupling coefficient (k) between antennas, several coil configurations have been designed and tested in order to show a wide range of cases. Measurements have been performed with three different coils. Each coil has been manufactured on two different substrates: FR4 and Ultralam 3000 (see Figure 1.22).

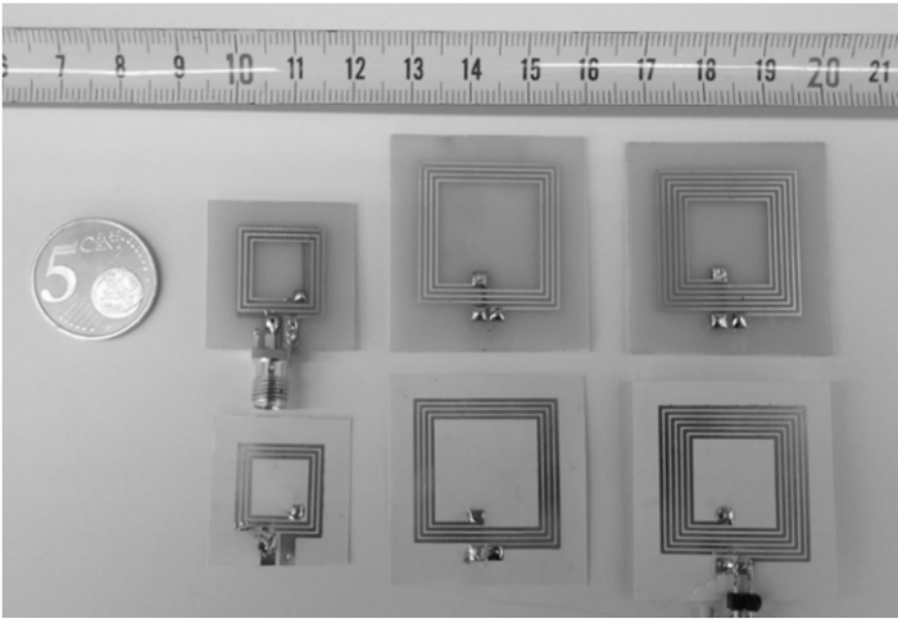

Figure 1.22. *Coils that have been designed and tested for characterizing the coupling coefficient. Coil 1 (left), coil 2 (center) and coil 3 (right). The three at the top are printed on the FR4 substrate and the three at the bottom in Ultralam. For a color version of this figure, see www.iste.co.uk/girbau/sensors.zip*

The main parameters of each coil antenna are shown in Table 1.3. Physical design parameters and measured electrical parameters are provided. Table 1.3 can be used to compare the influence of the substrate and to compare the behavior of identical coils when manufactured on the FR4 substrate versus a flexible substrate (i.e. Ultralam, UL).

	Coil 1		Coil 2		Coil 3	
	FR4	UL	FR4	UL	FR4	UL
Size (mm)	15×15		25×25		25×25	
Turns (N)	6		4		6	
Printed sides	2		1		1	
Trace width (mm)	0.7		0.7		0.7	
Spacing between traces (mm)	1		1		1	
Inductance (L_2, nH)	683	757	724	697	1182	1154
Resonance frequency (f_r, MHz)	106.33	66.57	115.83	130.29	96.69	104.31
Quality factor at 13.56 MHz (Q_2)	58.88	41.16	66.57	51.86	75.92	56.55
Antenna factor at 13.56 MHz (AF)	0.96	1.03	5.98	5.86	5.63	5.53

Table 1.3. *Coil parameters. Three different configurations, in two different substrates, FR4 and Ultralam (UL)*

Coil 1 in FR4 has been used as a reference coil, measuring the coupling coefficient (k) between this coil and the others. The results, shown in Figure 1.23, demonstrate that the best coupling is found when the two coils are identical (blue continuous line). When using the same configuration but with a different substrate (blue dashed line), a degradation on k is observed. However, when the two coils have different parameters (coils 2 and 3, red and orange lines, respectively), the difference between substrates (continuous line for FR4 and dashed line for Ultralam) is almost imperceptible.

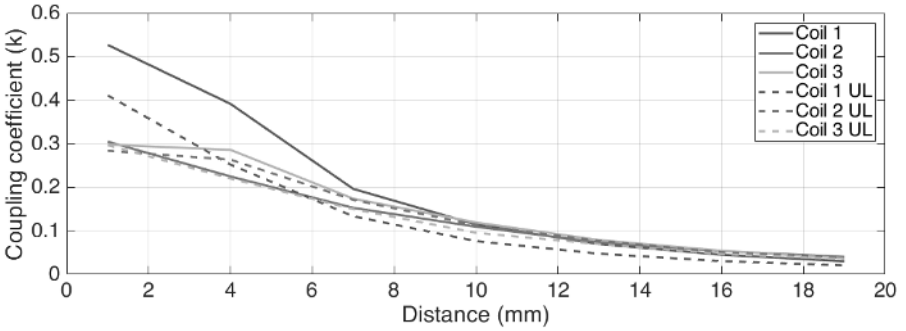

Figure 1.23. *Coupling coefficient (k) between coil 1 and six different coils. For a color version of this figure, see www.iste.co.uk/girbau/sensors.zip*

1.5.3. *Presence of metal near the antenna*

As explained in section 1.4.6, the presence of metal near the antenna produces undesirable effects. Figure 1.24 compares the measured inductance (L_2) and quality factor (Q_2) at 13.56 MHz as a function of the distance to a metallic plane that simulates the effect of metallic parts of the mobile phone. The coil antenna used for this test is a 50×50 mm with six loops, with a 0.7 mm trace width and space between traces of 1 mm. It is important to highlight that the inductance decreases when the loop antenna is close to metal, due to the induced image currents with opposite directions that reduce the magnetic flux. For distances longer than 15 mm, the inductance is nearly flat with an average value of around 1.8 µH. As the resonance frequency of the tag can be tuned adding a capacitor in parallel with the antenna, depending on the chosen value, the tag can be designed to improve its performance in ultra-short, short or long ranges. Usually, the selected distance for tuning is greater than 15 mm, because the coupling coefficient is lower than in the other cases and, therefore, the power received at the tag is expected to be higher as it is close to the smartphone.

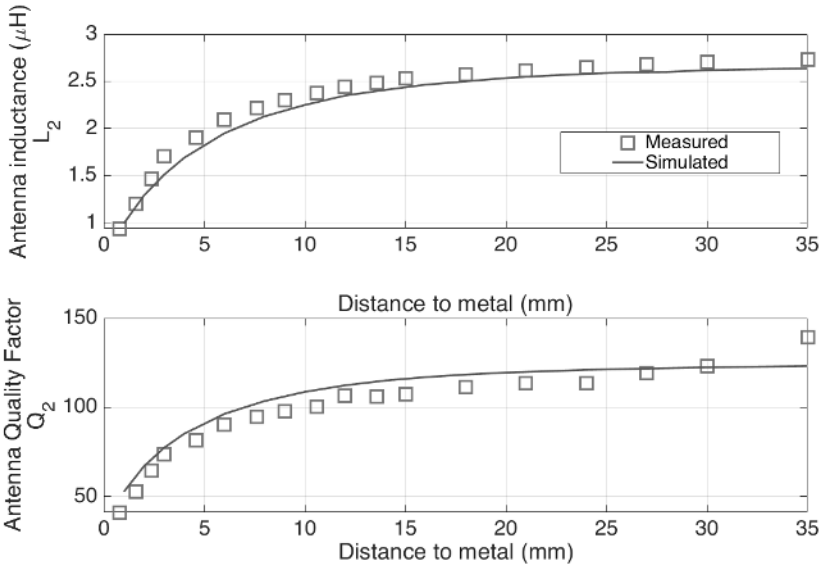

Figure 1.24. *Measured (□) and simulated (solid line) inductance (L_2) (a) and quality factor (Q_2) (b) of the loop antenna as a function of the distance to a metal plate. For a color version of this figure, see www.iste.co.uk/girbau/sensors.zip*

This effect at very short distances is compensated by the higher power received. The detuning of the antenna caused by the presence of metal is shown in Figure 1.25.

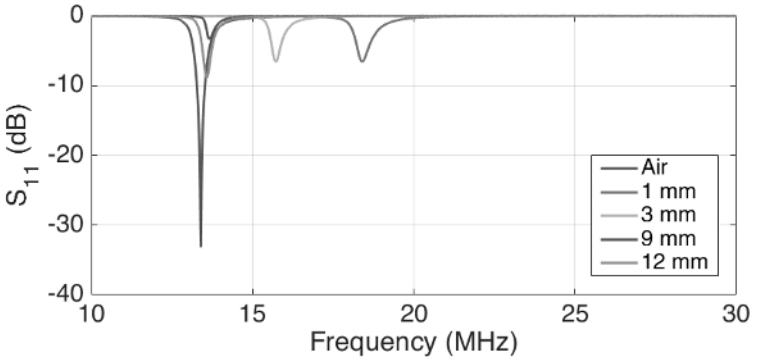

Figure 1.25. *Measured S_{11} of the antenna for different distances between the tag and the smartphone. For a color version of this figure, see www.iste.co.uk/girbau/sensors.zip*

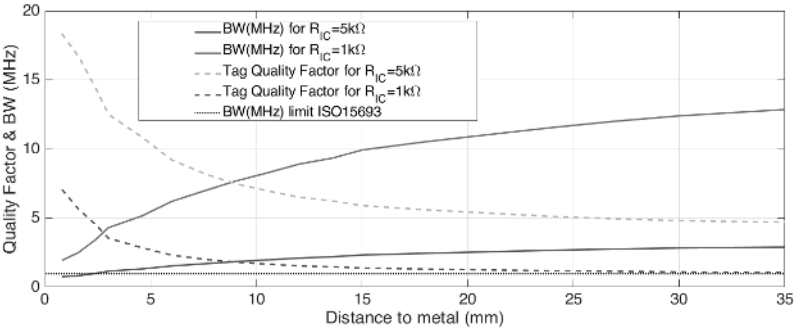

Figure 1.26. *Tag quality factor and bandwidth (BW) as a function of distance to metal depending on the IC resistance R_{IC}. The limit BW for ISO 15693 is also shown. For a color version of this figure, see www.iste.co.uk/girbau/sensors.zip*

In addition, when the tag is close to the smartphone, the bandwidth of the system increases because the tag quality factor decreases. This is caused both by the antenna quality factor reduction and by the decrease in the load resistance of the IC (due to higher power received at the tag). It is important to note that, due to power limitation of the standard VNA (often < 20 dBm), the field generated with the lab equipment is smaller than in a real reader, as is the measured field. Therefore, the IC impedance

(especially the equivalent resistance) is higher than in a real situation. The IC resistance decreases typically from R_{IC} = 5 kΩ to 1 kΩ under high power excitation when the tag is very close to the reader (Gvozdenovic *et al.* 2014). Therefore, the quality factor of the tag decreases, and the tag bandwidth (*BW*) increases. Figure 1.26 shows the quality factor and *BW* as a function of the tag to smartphone distance showing that the *BW* is higher than the required ISO/IEC 15,693 (968 kHz). The shape distortion is due to the metal present in the reader.

1.5.4. *Energy harvesting*

The average magnetic field (H_{av}) received at the NFC tag must be above a threshold value (H_{min}) for a correct conversion from RF to DC. H_{min} depends on the tag resonance frequency and is obtained as (Gebhart 2011):

$$H_{min} \approx \frac{\sqrt{\left[1-\left(\frac{f_{op}}{f_r}\right)^2\right]^2+\frac{1}{Q_{2L}^2}}}{2\pi f_{op}\mu_0 AN}\cdot U_{min} \qquad [1.32]$$

where U_{min} is the minimum voltage required for the tag operation, which depends on the IC design and technology. It is important to mention that H_{min} changes depend on the IC, since each IC has different U_{min} and resistance R_{IC}. H_{min} also depends on the coil size (A) and on the number of turns (N). Considering that the tag is tuned ($f_r = f_0$), and that $Q_L \ll Q_2$, then it can be considered that $Q_{2l} \approx Q_L = R_{IC}/\omega_0 L_a$. Thus, under these approximations, H_{min} can be estimated as:

$$H_{min} \approx \frac{1}{\omega_0\mu_0 A\cdot N}\cdot\frac{U_{min}}{R_{IC}}\cdot\omega_0 L_a = \frac{I_{min}}{\omega_0\mu_0}\cdot\left(\frac{L_a}{A\cdot N}\right) \qquad [1.33]$$

Hence, the minimum magnetic field to activate the EH depends on the minimum threshold current of each chip (I_{min}), and the antenna parameters (L_a, A, and N).

The average magnetic field (H_{av}) depends on the power transmitted by the reader and the coupling between the loop antennas (distance). On the other hand, H_{min} can be considered a figure of merit of the tag because it depends only on its parameters (IC and antenna). Therefore, it can be employed to evaluate the tag performance regardless of the reader used to generate the field. Figure 1.27 shows the calculated H_{min} considering Q_{2L} = 70, L_2 = 0.7 µH, A = 15×15 mm, N = 6 and U_{min} = 4.8V, for two different values of R_{IC} (450 Ω and 525 Ω) (Gvozdenovic *et al.* 2014).

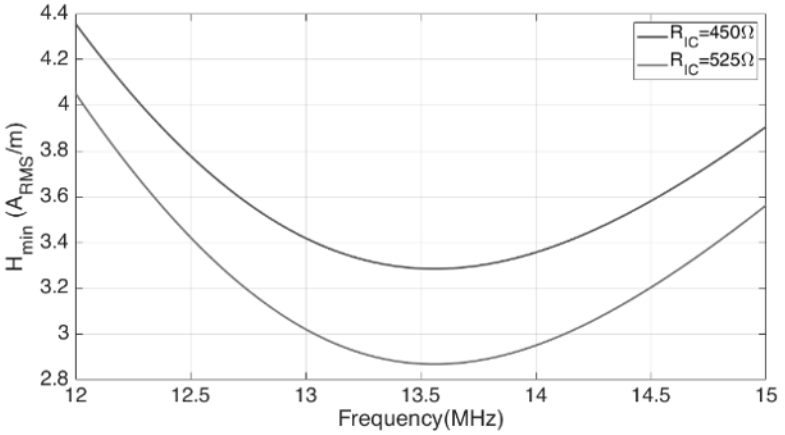

Figure 1.27. *Calculated minimum magnetic field* H_{min}*(*A_{RMS}/m*) as a function of the frequency. For a color version of this figure, see www.iste.co.uk/girbau/sensors.zip*

Figure 1.28 shows the H_{av} as a function of the distance for two smartphones. The measurements have been done with a tag on the FR4 substrate, with an antenna with six loops and an area of 50×50 mm (the same used in section 1.5.3) connected to an MR24LR NFC IC. The NFC IC is connected via an I^2C bus to a load consisting of an ATtiny85 microcontroller. Taking into account the current consumption of the tag, the reading range varies between 1 and 1.75 cm, depending on which smartphone is used as the reader. This distance corresponds to a measured minimum magnetic field (H_{min}) equal to 1.1 A_{RMS}/m (black dashed line in Figure 1.28). At the threshold distance, the measured power performed with the SA (that corresponds to the tag loaded with R_L = 50 Ω) is approximately 3 dBm. It can be seen that once the magnetic field drops below the threshold, the voltage output falls to zero (Boada *et al.* 2018b). Mobile 1 transmits higher power than mobile 2 (it is an older model) and consequently the read range is noticeably higher.

Another factor to be considered is the stability of the rectified voltage generated from the harvested energy. To ensure correct communication within the tag, Figure 1.29(a) shows the energy harvested when illuminated with a smartphone, and Figure 1.29(b) shows the data communication between the microcontroller, the tag and the sensors using the I^2C protocol. The result shows the viability of using digital communication while being powered up by the reader.

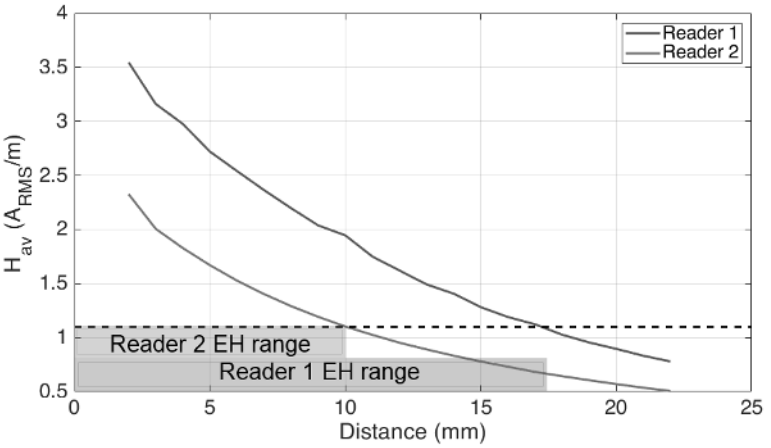

Figure 1.28. *Measured average magnetic field as a function of the tag-to-reader distance for two mobile models. For a color version of this figure, see www.iste.co.uk/girbau/sensors.zip*

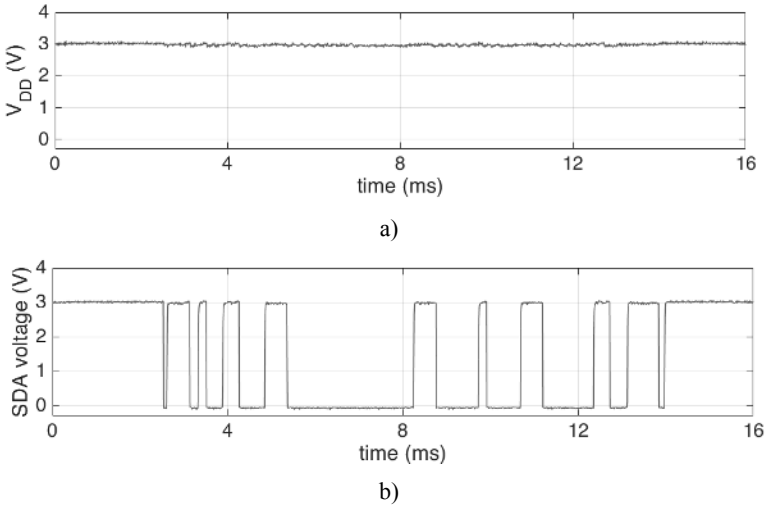

Figure 1.29. *Measurement of the energy-harvesting output (V_{DD}) (a) and the data of the SDA line from the I^2C bus (b) when the tag is powered by the NFC reader. For a color version of this figure, see www.iste.co.uk/girbau/sensors.zip*

1.5.5. *Backscattering measurement*

When a tag is powered up by receiving a magnetic field generated by the reader (H_{av}), it modulates the amplitude of the carrier frequency (f_o) with the information contained in the NFC IC memory. This modulation produces two sidebands that contain the information. Even though the correct reception of the information can be checked on the reader after reading the information, it is interesting to analyze the power of this sideband as they are the signals to be demodulated at the reader to retrieve the information. In order to measure it without affecting communication, a test coil is placed behind the tag at a distance of 10 mm, connected to an SA (Figure 1.30). Since the tag emits in both perpendicular directions symmetrically (forwards and backwards), the test antenna receives a signal very similar to the signal received at the reader.

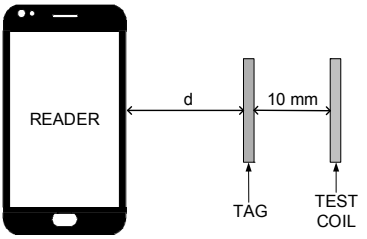

Figure 1.30. *Setup for backscattering measurement. For a color version of this figure, see www.iste.co.uk/girbau/sensors.zip*

Figure 1.31 shows the measured spectrum when the distance between the reader and tag (d) is 10 mm. The center (carrier) frequency is located at 13.56 MHz and the sidebands have a deviation of ± 424 kHz referred to the carrier (tags based on the ISO/IEC 15693 standard, where $f_{sidebands} = f_o \pm f_o/32$). The setup used for this test integrates a Xioami Mi Note 2 as the reader, and a tag based on an M24LR04 NFC IC, with a 15×15 mm coil antenna (coil 1 in Table 1.3).

The measured power of the carrier, of the lower and the upper sidebands as a function of distance is shown in Figure 1.31. It can be observed that the sidebands have different levels of power, which is because the resonance frequency (f_r) is not exactly centered at 13.56 MHz, but at a slightly lower frequency. Furthermore, at very short distances, the sidebands are hugely degraded due to the reduction of the chip resistance under high power excitation. The sideband power for the presented setup is under the noise floor for distances longer than 25 mm.

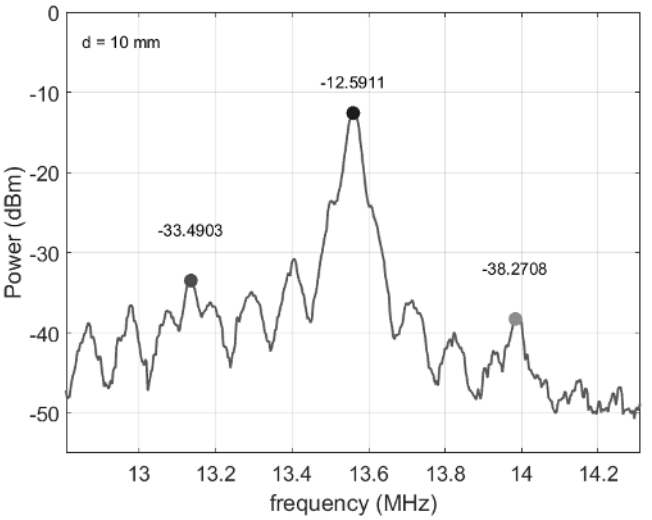

Figure 1.31. *Spectrum of the signal generated by the tag, at a 10 mm separation between the reader and tag. For a color version of this figure, see www.iste.co.uk/girbau/sensors.zip*

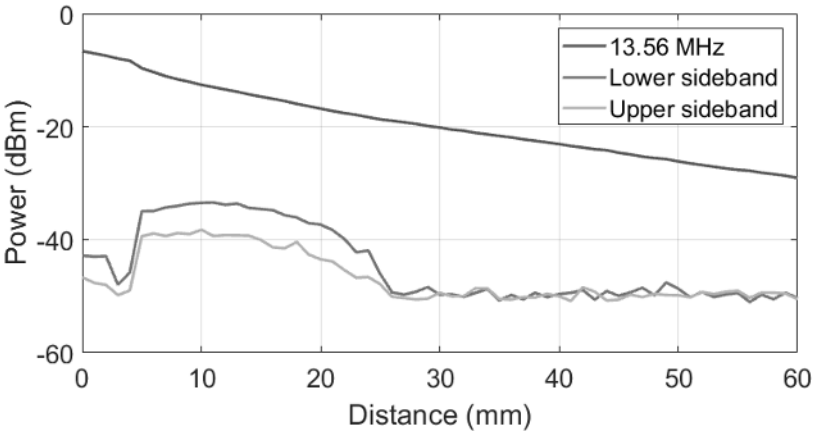

Figure 1.32. *Measured power of the carrier frequency (blue) and the sidebands (red and orange) as a function of the distance. For a color version of this figure, see www.iste.co.uk/girbau/sensors.zip*

1.5.6. *NFC IC comparison*

This section presents viable options for developing applications in real-life scenarios, hence the importance of analyzing and comparing the current, commercially available NFC IC. Table 1.4 shows a comparison of some selected NFC ICs with EH capability, providing information on the maximum current available and the typical voltage supplied after AC–DC rectification.

Manufacturer	IC model	EH max. current (mA)	Typical voltage (V)	Standard (ISO/IEC)
ST Microelectronics	M24LR-E-R (ST Microelectronics 2017b)	6	3	15,693
	ST25DV-12C (ST Microelectronics 2017a)	6	3	15,693
NXP	NT3H1101 (NXP Semiconductors 2015a)	5	2	14,443A
	NT3H1201 (NXP Semiconductors 2015b)	5	2	14,443A
EM Microelectronics	NF4 (EM Microelectronics 2014)	5	3.6	14,443A
Giantec Semiconductor	GT23SC6699 (Giantec Semiconductor 2011)	NA	3.2	14,443A
Silicon Craft	SIC4310 (Silicon Craft 2014a)	10	3.3	14,443A
	SIC4340 (Silicon Craft 2014b)	10	3.3	14,443A
	SIC4341 (Silicon Craft 2014c)	10	3.3	14,443A
AMS AG	AS3953 (AMS 2013)	5	2	14,443A
	SL13 (AMS 2014)	4	3.4	15,693
Melexis	MLX90129 (MELEXIS 2012)	5	3	15,693
Texas Instruments	RF430FRL152H (Texas Instruments 2014a)	NA	3	15,693

Table 1.4. *Comparison of NFC ICs with energy harvesting (Lazaro* et al. *2018)*

In order to perform a representative NFC IC comparison and introduce the ICs used in the tags shown in the following chapters, three different models of NFC IC

with EH capability have been analyzed: two chips from ST Microelectronics (ST25DV04k (ST Microelectronics 2017a) and M24LR04E (ST Microelectronics, 2017b), both based on NFC Forum type tag 5, NFC-V, ISO/IEC 15693) and the others from NXP Semiconductors (NT3H1101 (NXP Semiconductors 2015a), type tag 2, NFC-A, ISO/IEC 14443A). For the sake of simplicity, these chips will now be referred to as ST25, M24 and NT3H, respectively. In order to compare the three ICs, they have been integrated in the same tag (see Figure 1.33). The tag integrates a 50×50 mm square loop antenna printed on FR4 (thickness 0.8 mm, metallization thickness 34 μm). The antenna has six loops, with a width of 0.7 mm and gaps of 1 mm. In all cases, the NFC IC is connected via an I^2C bus to an ATtiny85 microcontroller (Atmel 2014) programmed with the same code, which consists of a counting loop with the purpose of having the same exact load.

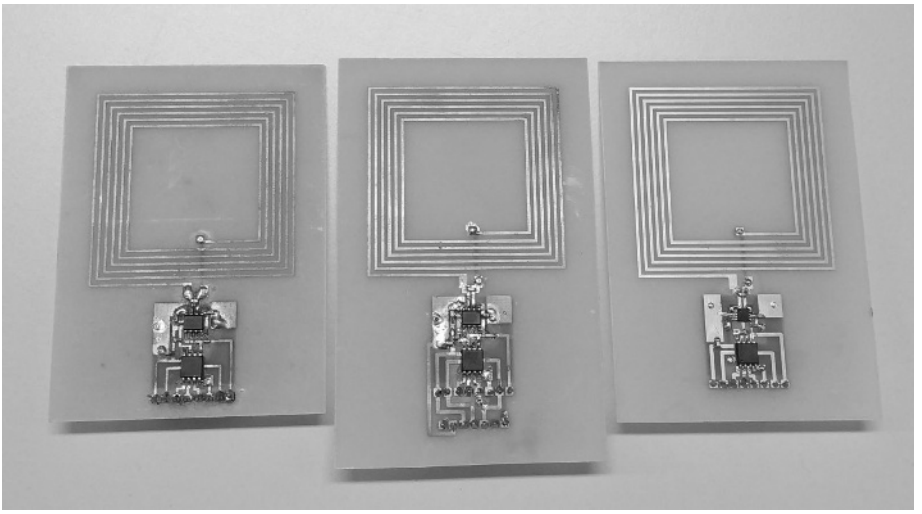

Figure 1.33. *Same tag with three different chips. M24 (left), ST25 (center) and NT3H (right). For a color version of this figure, see www.iste.co.uk/girbau/sensors.zip*

To determine the performance of each chip, the RMS voltage at the antenna terminals (V_{ant}) and the rectified voltage from the RF signal (V_{DD}) have been measured as a function of the distance between the reader and tag, using an oscilloscope with a low-capacitance probe. Figure 1.34 shows these two parameters for each of the ICs. Measurements have been carried out with two different smartphones, a Xiaomi Mi Note 2 (Figure 1.34(a)) and a BQ Aquarius V (Figure 1.34(b)). Since each manufacturer uses different antennas and different ICs

as a transceiver, the power emitted by the reader, the coupling between the reader and tag, and the received magnetic field change between them. Hence, the importance of measuring the parameters using different smartphones as an interrogator.

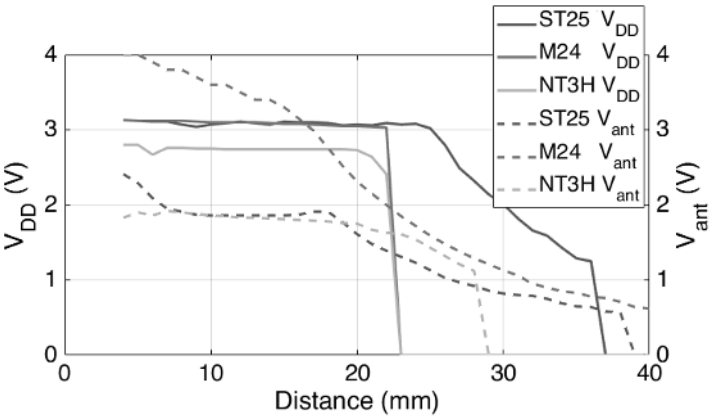

a)

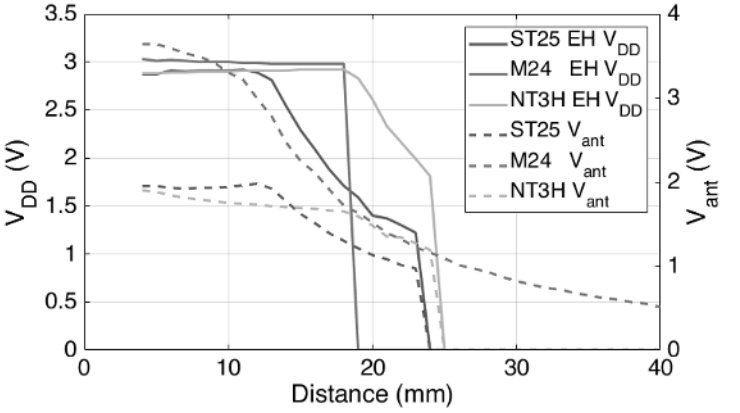

b)

Figure 1.34. *Rectified energy-harvesting output of the chip (V_{DD}, continuous line) and voltage at the antenna terminals (V_{ant}, dashed line) for different distances. Measured with two different smartphones: (a) Xiaomi mi Note 2 and (b) BQ Aquarius V. For a color version of this figure, see www.iste.co.uk/girbau/sensors.zip*

Analyzing the parameter V_{DD} (continuous line), the ST25 has a longer range; however, after a certain point (25 mm in (a), 13 mm in (b)), the output voltage degrades progressively, whereas in the case of the other two chips, an ON–OFF behavior is observed, going from about 3 V when active to 0 V abruptly. This fact might be a benefit depending on the application. For instance, some types of sensors require a certain voltage to work properly, and a smooth decrease in V_{DD} (seen in the case of the ST25 in Figure 1.34) can cause a malfunction that leads to an incorrect reading. A steep decrease of the voltage at the antenna terminals to zero (V_{ant}, dashed line) is observed with the ST25 and the NT3H. This is the result of a battery-saving operational mode of the NFC readers, which consists of sending periodic short pulses to detect the tag. If the reader cannot demodulate the answer from the backscattered sidebands of such a pulse then it stops transmitting, which means it does not detect any tag. In order to detect a nearby tag, a discovery pulse is generated every few seconds and, if detected, the pulse is held at the operating frequency, generating the voltage at the antenna terminals. Figure 1.35 depicts the signals generated by the reader to detect the tag. The graphic at the top shows the scene in the absence of the tag; approximately every 2 seconds, the reader emits a signal modulated with the different discovery requests of each supported standard. As an example, the bottom graphics of Figure 1.35 show the request modulation for NFC-B (ISO/IEC 14443B, bottom-left, using 10% ASK modulation), and for NFC-V (ISO/IEC 15693, bottom-right, using 100% ASK modulation). In the case presented in Figure 1.35, the reader has full NFC capability; therefore, the request messages for NFC-A (ISO/IEC 14443A) and NFC-F (JIS X6319) are present, as well within the discovery messages (middle-left image in Figure 1.35). This burst of requests lasts approximately 50 ms and includes polling requests of a few milliseconds each, followed by a period of unmodulated carrier to send the energy to the tag while waiting for an answer. In the midst of every attempt of polling a new tag, the reader generates short signals of the carrier frequency without modulation, shown in the middle-right image in Figure 1.35, of around 125 μs. These signals are required by the standards, and the purpose is to ensure that a listening device (i.e. a tag) will be correctly reset by a polling device (i.e. a reader), which is emitting the worst-case residual carrier level.

When the reader does not detect the presence of the tag, it keeps sending these bursts of requests, which generates a sporadic voltage at the antenna terminals (V_{ant}), but if the reader does not detect the answer to the request, it will not start sending a constant signal. Therefore, the NFC IC would not provide the rectified voltage to power up the tag. Consequently, when the voltage at the antenna terminals (Vant) maintains a value greater than zero, the reader detects the tag, even when the magnetic field intensity is below the minimum threshold required to activate the rectified voltage output of the NFC IC.

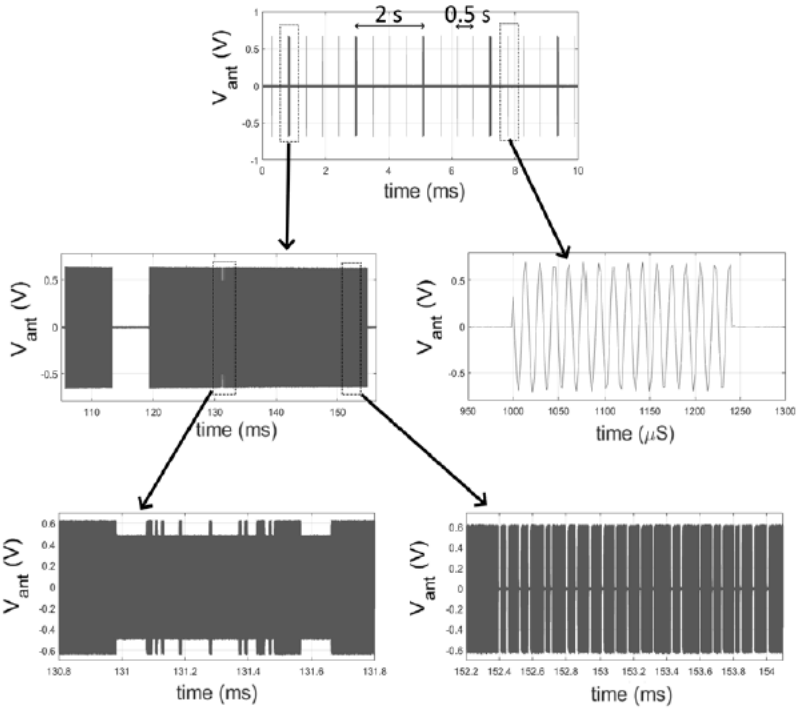

Figure 1.35. *Discovery signals sent by the reader when no tag is present. For a color version of this figure, see www.iste.co.uk/girbau/sensors.zip*

1.5.6.1. *Effects of the loads*

In order to compare the load effect at the output of the NFC IC (V_{DD}), the tags shown in Figure 1.33 have been modified, removing the MCU and connecting resistors instead. Figure 1.36 shows the measurements obtained for the M24 (Figure 1.36(a)), the ST25 (Figure 1.36(b)) and the NT3H (Figure 1.36(c)). The reader used for these measurements is a Xiaomi Mi Note 2.

Figure 1.36 shows the energy that NFC ICs can provide as a function of distance for different loads connected to their output. The smaller the load, the shorter the maximum distance and the supplied power. Considering the smallest load in this setup (510 Ω), the M24 can provide around 14 mW for distances up to 14 mm, the ST25 12 mW up to 18 mm and the NT3H 12 mW up to 20 mm. On the other hand, when connecting a 10 kΩ load, the M24 gives 1 mW up to 21 mm, the ST25 1.07 mW up to 30 mm and the NT3H 0.9 mW up to 47 mm.

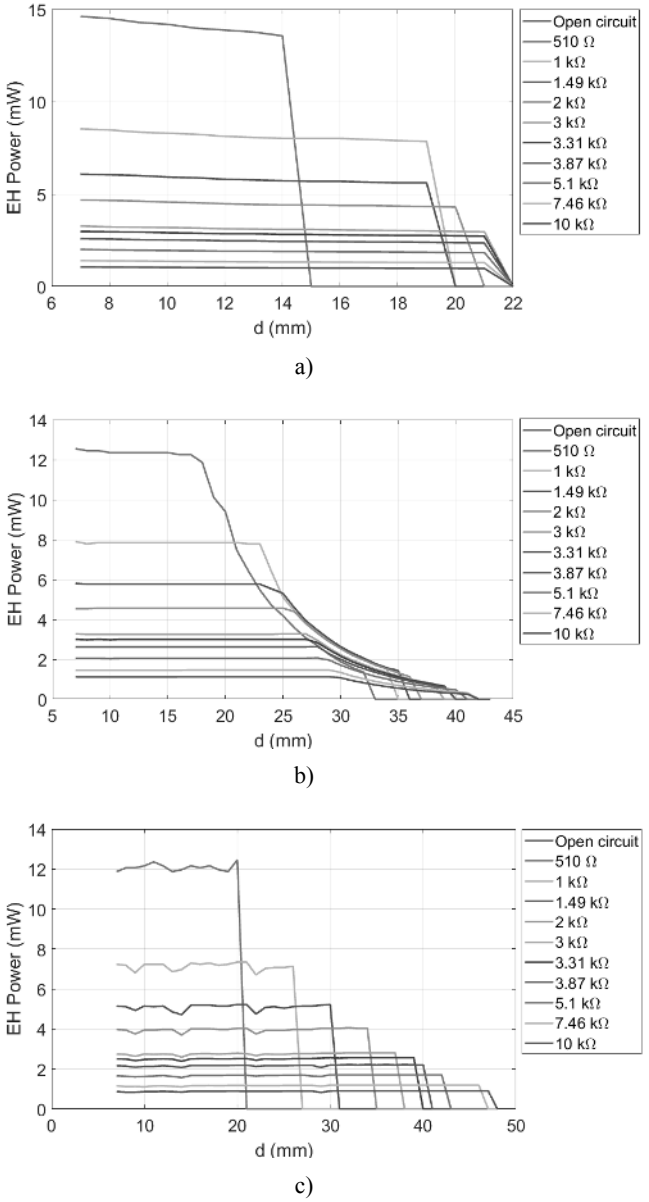

Figure 1.36. *Power harvested for different loads, with different NFC ICs. (a) M24; (b) ST25; and (c) NT3H. All the tags have a 50×50 mm six-loop antenna, and a Xiaomi Mi Note 2 is used as a reader. For a color version of this figure, see www.iste.co.uk/girbau/sensors.zip*

Figure 1.37 shows the supplied power depending on the load connected, for a distance of 14 mm between the reader and tag. It can be seen that the power decreases abruptly for loads between 0.5 kΩ and 2 kΩ, going from around 12 mW at 500 Ω to 4 mW at 2 kΩ.

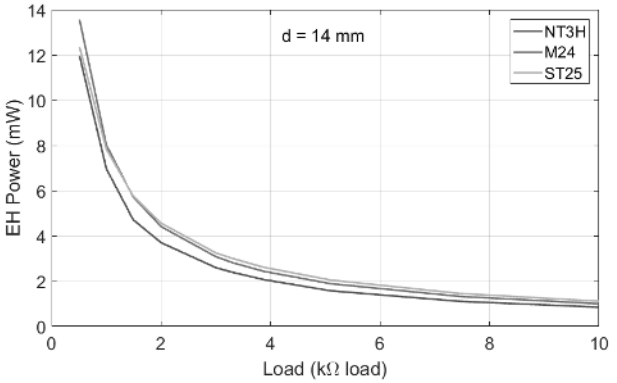

Figure 1.37. *Power at the rectified output for the M24, ST25 and NT3H ICs as a function of the load connected, at a distance of 14 mm between the reader and tag. For a color version of this figure, see www.iste.co.uk/girbau/sensors.zip*

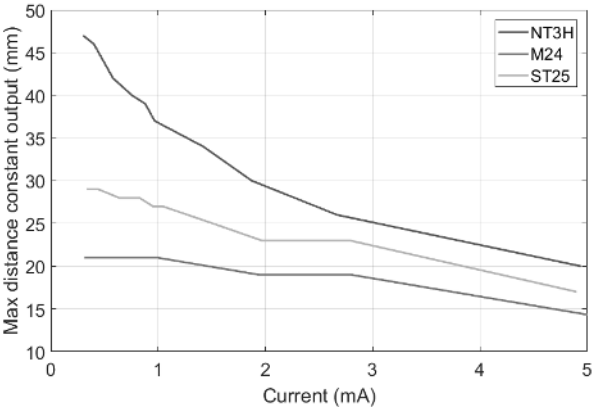

Figure 1.38. *Maximum distance at which the NFC ICs can supply a constant current for different loads for the NT3H (blue), the M24 (red) and the ST25 (yellow). For a color version of this figure, see www.iste.co.uk/girbau/sensors.zip*

From Figure 1.36, it has been deduced that the power supplied by the ICs is almost constant up to a certain point at which it drops to zero. The maximum distance at which the chips can supply certain current is shown in Figure 1.38. The NT3H IC has a longer range for identical current supply than the other two ICs. It is also the one whose current experiences greater variation with distance, since from 5 mA to 0.3 mA, it has 27 cm of difference (from 20 to 47 cm), whereas the ST25 has a 12 mm difference (from 17 to 29 mm) and the M24, 7 mm (from 14 to 21 mm).

1.5.7. *Antenna dimensions*

As mentioned previously, NFC has a wide range of possible applications. In some of those applications, the size of the tag does not matter, but in other applications, the size is essential (e.g. implantable tags). Hence, the importance of evaluating the differences between using a large or a small antenna. For this study, two antennas are compared. The first one is a 50×50 mm coil (Figure 1.39(a)), and the second is a 15×15 mm coil (Figure 1.39(b)), both with six turns (in the 15×15 mm antenna, three turns in each face of the PCB).

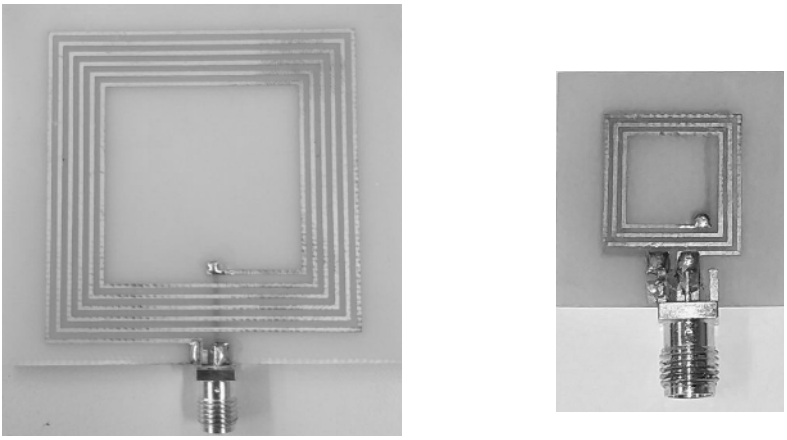

a) b)

Figure 1.39. *(a) Coil antenna with six loops printed on one side and an area of 50×50 mm and (b) coil antenna with six loops (double-sided) and an area of 15×15 mm. For a color version of this figure, see www.iste.co.uk/girbau/sensors.zip*

Figure 1.40 plots the power and the average magnetic field received in these antennas using a Xiaomi Mi Note 2 as a reader. The power is slightly higher in the case of the larger antenna because its size is closer to the size of the reader's antenna, a situation that optimizes the received power. On the other hand, the

average magnetic field is higher for the smallest antenna, since, as outlined in section 1.4.5, the received magnetic field (H_{av}) depends on the AF, and the AF (defined in equation [1.19]) increases when the area of the antenna (A) decreases.

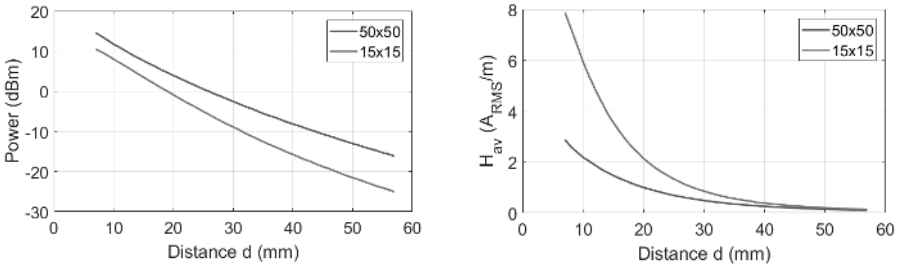

a) b)

Figure 1.40. *Comparison of (a) power and (b) magnetic field received by a 50×50 mm coil antenna (blue line) and a 15×15 mm coil antenna (red line). For a color version of this figure, see www.iste.co.uk/girbau/sensors.zip*

To compare the effects of the antenna size for the three NFC ICs analyzed in the previous section, the same three tags with small antenna of 15×15 mm have been made (Figure 1.41).

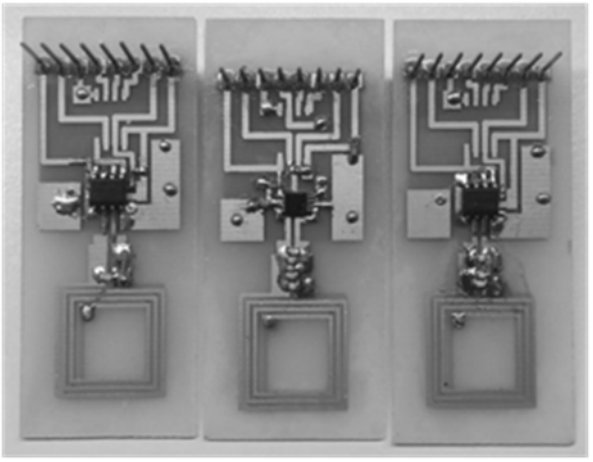

Figure 1.41. *Same tag with three different chips. M24 (left), NT3H (center) and ST25 (right) with a 15×15 mm antenna. For a color version of this figure, see www.iste.co.uk/girbau/sensors.zip*

Each tag consists of the antenna connected to the NFC chip, with a 3 kΩ resistor as a load which leads to 1 mA, approximately. Figure 1.42 displays the measured voltage at the load for each tag using a Xioami Mi Note 2 as a reader. The results show that the M24 (red) and the ST25 (orange) have almost the same behavior with antennas of two different sizes; however, the NT3H reduces its range by 1 cm (from 38 mm to 28 mm) when using the small antenna.

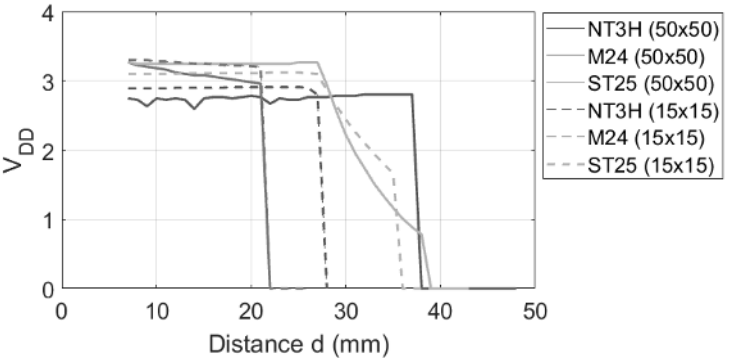

Figure 1.42. *Measured voltage (V_{DD}) for three different ICs (NT3H blue, M24 red and ST25 orange), with a 50×50 mm antenna (continuous line) and a 15×15 mm antenna (dashed line), with a 3 kΩ load. For a color version of this figure, see www.iste.co.uk/girbau/sensors.zip*

The maximum distance at which the EH is activated is obtained from the measurements shown in Figure 1.42. With those distances, and using the measurements shown in Figure 1.40(b), as well as taking into account the calculations explained in section 1.5.4, the H_{min} for each case can be estimated. The relationship between the H_{min} of the two antennas is derived from equation [1.33] and is expressed as:

$$\frac{H_{min}'}{H_{min}} = \frac{(L_2'/A'N')}{(L_2/AN)} \qquad [1.34]$$

where H_{min} and H_{min}' represent the magnetic field threshold to activate the EH output of the compared antennas. Using the values of each antenna, summarized in Table 1.5, the expected ratio between the H_{min} of these two antennas is around 1.7. However, this is a theoretical value, and the real measurements give ratios of 2.1 for the M24, 1.8 for the ST25 and 3.7 for the NT3H. The difference between the theoretical and measured values is due to different factors. The misalignment between coils during the experimental measurements could lead to a mismatch between the H_{av} measured with the test coil and the H_{av} received by the tag.

In addition, even though the resonance frequency (f_r) has been carefully adjusted using the VNA, a possible factor that could induce the difference between the theoretical and the measured values is the antenna tuning, since equation [1.34] assumes that f_r is equal to the operational frequency (f_0).

	Coil antenna 50×50 mm			**Coil antenna 15×15 mm**		
	M24	**ST25**	**NT3H**	**M24**	**ST25**	**NT3H**
Area (A, mm^2)	50			15		
Turns (N)	6			6		
Inductance (L, µH)	2.74			0.683		
Minimum magnetic field ($Hmin$, A_{RMS}/m)	0.93	0.6	0.31	1.94	1.1	1.22

Table 1.5. *Comparison of* H_{min} *with three different ICs for two antennas*